PCCP

Accepted Manuscript

ROYAL SOCIETY OF CHEMISTRY

www.rsc.org/pccp

PCCP

RSCPublishing

ARTICLE

Reversibility and two state behaviour in the thermal unfolding of oligomeric TIM barrel proteins†

Cite this: DOI: 10.1039/x0xx00000x

Sergio Romero-Romero[1], Miguel Costas[2], Adela Rodríguez-Romero[3] and D. Alejandro Fernández-Velasco[*1]

Received 00th XX,
Accepted 00th XX

DOI: 10.1039/x0xx00000x

www.rsc.org/

Temperature is one of the main variables that modulate protein function and stability. Thermodynamic studies of oligomeric proteins, the dominant protein natural form, have been often hampered because irreversible aggregation and/or slow reactions are common. There are no reports on the reversible equilibrium thermal unfolding of proteins composed by $(\beta/\alpha)_8$ barrel subunits, albeit this "TIM barrel" topology is one of the most abundant and versatile in nature. We studied the eponymous TIM barrel, Triosephosphate Isomerase (TIM), belonging to five species of different bacterial taxa. All of them were found to be catalytic efficient dimers. The three-dimensional structure of four enzymes were solved at high/medium resolution. Irreversibility and kinetic control were observed in the thermal unfolding of two TIMs, while for the other three the thermal unfolding was found to follow a two-state equilibrium reversible process. Shifts in the global stability curves of these three proteins are related to organismal temperature range of optimal growth and modulated by variations in maximum stability temperature and in the enthalpy change at that temperature. Reversibility appears to correlate with low isoelectric point, the absence of residual structure in the unfolded state, small cavity volume in the native state, low conformational stability and a low melting temperature. Furthermore, the strong coupling between dimer dissociation and monomer unfolding may reduce aggregation and favour reversibility. It is therefore very thought-provoking to find that a common topological ensamble, such as the TIM barrel, can unfold/refold in the Anfinsen way, *i.e.* without the help of the cellular machinery.

1. Introduction

The study of protein-folding has evolved during the last 50 years to become a mature research field.[1] Although the folding pathway of several proteins is being studied at atomic resolution and several de novo proteins have been designed,[2-4] our current understanding of the sequence/structure/stability relationship of proteins is limited by the information available in these different levels. The current number of protein sequences deposited in the GenBank[5] ($\approx 10^8$), is several orders of magnitude higher than the number of structures deposited in the Protein Data Bank (PDB)[6] ($\approx 10^5$). Likewise, the number of protein three-dimensional structures in the PDB is much bigger than their number in the Protein Stability Database[7] ($\approx 10^3$).

The evaluation of protein stability requires the use of a perturbant. Temperature and chaotropes such as guanidine hydrochloride (GndHCl) and urea are the main perturbants employed.[8] The characterization of the thermal unfolding transition gives a full description of the thermodynamic parameters that govern protein stability.[9,10] Irrespectively of the perturbant used to promote unfolding, the two prerequisites for the estimation of thermodynamic parameters are the reversibility of the process and that the system reaches equilibrium. These experimental requirements have limited the number of available data, particularly for medium and large monomeric and oligomeric proteins.[11] Although our current understanding of protein folding is based on small, single domain, monomeric and marginally stable systems,[12] oligomers account for at least 80% of the proteins in living cells.[13] One of the most common protein architectures, found mainly in oligomers but also in monomeric proteins, is the TIM barrel fold, observed in 10% of the proteins deposited in the PDB.[14] This $(\beta/\alpha)_8$ fold is composed by eight β strands that form a central β barrel surrounded by eight α helices. This common architecture has been found in many different proteins with various functions.[15,16] The Gnd-HCl and urea-induced unfolding of several monomeric TIM barrels has been studied in detail;[17-19] in contrast, there are only three reports on

Table 1. Physicochemical characterization of bacterial TIM.

TIM	Catalytic parameters for GAP isomerization[a]			Hydrodynamic and spectroscopic properties			Predicted secondary structure content[c] (%)				K_{diss}[d] (M)	T_m[e] (ºC)
	K_m (mM)	k_{cat} (s^{-1})	Catalytic efficiency[b] (M^{-1} s^{-1})	Stokes radius[a] (Å)	λ_{Max} (nm)	SCM (nm)	α-helix	β-strand	β-turn	Random coil		
Np TIM	0.51 ± 0.04	1736 ± 42	(8.63 ± 0.29) x 10^7	31.4 ± 0.7	331	342.1	36.1 ± 0.6	15.1 ± 0.5	16.3 ± 0.2	32.6 ± 0.8	(5.6 ± 0.7) x 10^{-8}	55.2 ± 0.4
Go TIM	0.34 ± 0.02	1306 ± 27	(9.51 ± 0.14) x 10^7	31.7 ± 0.8	325	339.5	31.4 ± 1.7	16.8 ± 0.8	15.8 ± 0.5	35.1 ± 0.5	(1.1 ± 0.2) x 10^{-7}	65.6 ± 0.5
Dr TIM	0.69 ± 0.03	5678 ± 84	(2.06 ± 0.18) x 10^8	31.6 ± 0.9	324	337.7	33.3 ± 0.9	16.3 ± 0.7	16.2 ± 0.3	34.3 ± 1.1	(1.4 ± 0.5) x 10^{-7}	44.6 ± 0.1
Sc TIM	0.74 ± 0.02	5668 ± 62	(1.93 ± 0.06) x 10^8	31.9 ± 0.6	325	339.5	41.3 ± 1.0	13.3 ± 0.9	15.7 ± 0.4	29.7 ± 0.7	(1.82 ± 0.5) x 10^{-7}	45.3 ± 0.2
Cp TIM	0.72 ± 0.04	6348 ± 127	(2.24 ± 0.10) x 10^8	32.1 ± 0.6	326	339.4	33.9 ± 1.9	16.5 ± 0.8	16.8 ± 0.4	32.8 ± 1.4	(2.9 ± 0.3) x 10^{-8}	58.3 ± 0.1

[a] Errors are the standard deviation of three different experiments.

[b] Catalytic efficiency was calculated from k_{cat}/K_m with the K_m value having been adjusted by the appropriate ratio (1:29) considering that only 4% of GAP in aqueous solution is the unhydrated aldehyde substrate, the only form that TIM is able to catalyze.[61]

[c] CD spectra was analyzed with CDNN[62], CDPro[63] and DichroWeb[64] to calculate the contributions of the various components to the protein secondary structure. Reported errors are an average of the deviations obtained using the three different software packages.

[d] Fitted to the dilution experiments at 25 °C using eqn (1) (Fig. 1). For *Np*TIM and *Go*TIM K_{diss} are apparent K_{diss} since the process is irreversible. Errors are derived from data fitting.

[e] Average value of the CD and DSC experiments with protein concentration of 15 μM and scan rate 1.0 K min^{-1}. Errors are the standard deviation of CD and DSC experiments.

the reversible temperature-induced unfolding of monomeric TIM barrels[20-22] and none describing an oligomeric TIM barrel. The only oligomeric TIM barrel with a reversible chaotrope-induced unfolding transition so far characterized is Triosephosphate Isomerase, the first protein where the TIM barrel fold was found.[23-38]

Triosephosphate isomerase (E. C. 5.3.1.1) (TIM) is a key glycolytic enzyme that catalyzes the isomerization of glyceraldehyde-3-phosphate (GAP) and dihydroxyacetone phosphate (DHAP).[39,40] TIM is an obligated homooligomer, with monomers structured in the canonical $(\beta/\alpha)_8$ barrel. The three-dimensional structures and catalytic properties of TIM from different species are quite similar.[41,42] In contrast, the unfolding pathway of TIM from different organisms is very diverse. Chaotrope-induced unfolding transitions have been described by models which increase in complexity from two-state to multistate reactions that involve monomeric and/or dimeric intermediates.[23-38] Regarding thermal unfolding, eighteen TIMs, mainly from eukaryotes, as diverse as Amoebozoa, Euglenozoa, Ascomycota and Chordata, have been studied. Even though a full thermodynamic characterization has been hampered by irreversible aggregation and/or the presence of hysteresis in all of them,[36,38,43-53] the activation parameters that describe the kinetic control of five eukaryotic TIMs have been reported.[52,53]

Although species from the bacteria domain are abundant and widely distributed in a variety of environmental conditions, bacterial TIMs have been much less studied than eukaryotic TIMs despite their biomedical or biotechnological importance. In this work, we characterized the structure, catalytic properties, association state and temperature-induced unfolding of five bacterial TIMs representatives of different supertaxa or clades that comprise different stages of bacterial evolution.[54] They were the TIMs of *Deinococcus radiodurans* (*Dr*TIM) from Hadobacteria, of *Nostoc punctiforme* (*Np*TIM) from Cyanobacteria, of *Gemmata obscuriglobus* (*Go*TIM) from Gracilicutes, of *Clostridium perfringens* (*Cp*TIM) from Endobacteria and of *Streptomyces coelicolor* (*Sc*TIM) from Actinobacteria (Fig. S1, ESI†). Here, we studied their thermal unfolding finding that two of them present kinetic control whereas for the other three, the presence of reversible transitions allowed an equilibrium thermodynamic analysis. Furthermore, the three-dimensional structures of four of these enzymes were solved at high/medium resolution and a structural analysis was performed to explore the possible relation between molecular level properties and reversibility.

2. Results and discussion

2.1 Biochemical characterization

The five recombinant proteins characterized in this work were purified to homogeneity with high yields (see Materials and Methods). Their far UV-Circular Dichroism (CD) native spectra showed minima at 210 and 220 nm (Fig S2, ESI†), a characteristic feature of β/α proteins. The λ_{max} and SCM of their intrinsic fluorescence spectra are (Table 1 and Fig. S3, ESI†) in the range found in many native proteins.[55] As previously observed in other wild type TIMs, catalytic activity measurements were well-fitted by the Michaelis-Menten equation and catalytic efficiency values were near the diffusion-limited behaviour (Table 1). Size Exclusion Chromatography (SEC) experiments indicate that BacTIMs show the Stoke´s radius expected for a compact dimer (Table 1); however, at a lower protein concentration (in the 0.5-5.0 μM range), catalytic

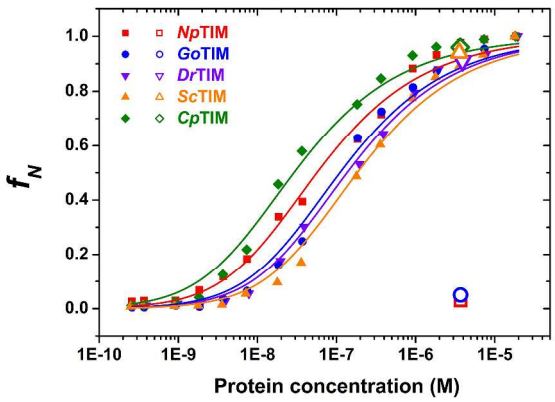

Fig. 1. Fraction of active TIM molecules as a function of protein concentration at 25 ºC. Solid curves show the best fit of experimental data (closed symbols) to a dissociation model (eqn (1)). For the reversibility test (open symbols), samples were incubated at 2 x 10^{-9} M for 48 hours and then concentrated to 4 x 10-6 M prior to catalytic activity measurements.

activity decreased in a concentration dependent way, the signature of a dissociation process to inactive monomers (Fig. 1). For *Dr*TIM, *Sc*TIM and *Cp*TIM dissociation was a reversible process; in contrast, for *Go*TIM and *Np*TIM activity was not recovered after the samples were concentrated (Fig. 1). From these experiments the dimer dissociation constants were calculated. The obtained values (30 to 180 nM; Table 1), are similar to those reported for eukaryotic TIMs (EukTIMs).[56-60]

2.2 Kinetic control in the thermal unfolding of *Np*TIM and *Go*TIM

The temperature-induced unfolding of BacTIMs was then studied. The native CD spectra of *Np*TIM and *Go*TIM was not recovered after heating the samples to 75 °C and cooling back to 25 °C, protein aggregation in the CD cell was observed, and there was no recovery of enzyme activity. Hence, the temperature-induced unfolding of these two proteins is irreversible. Differential Scanning Calorimetry (DSC) was then used to determine the activation parameters that describe the

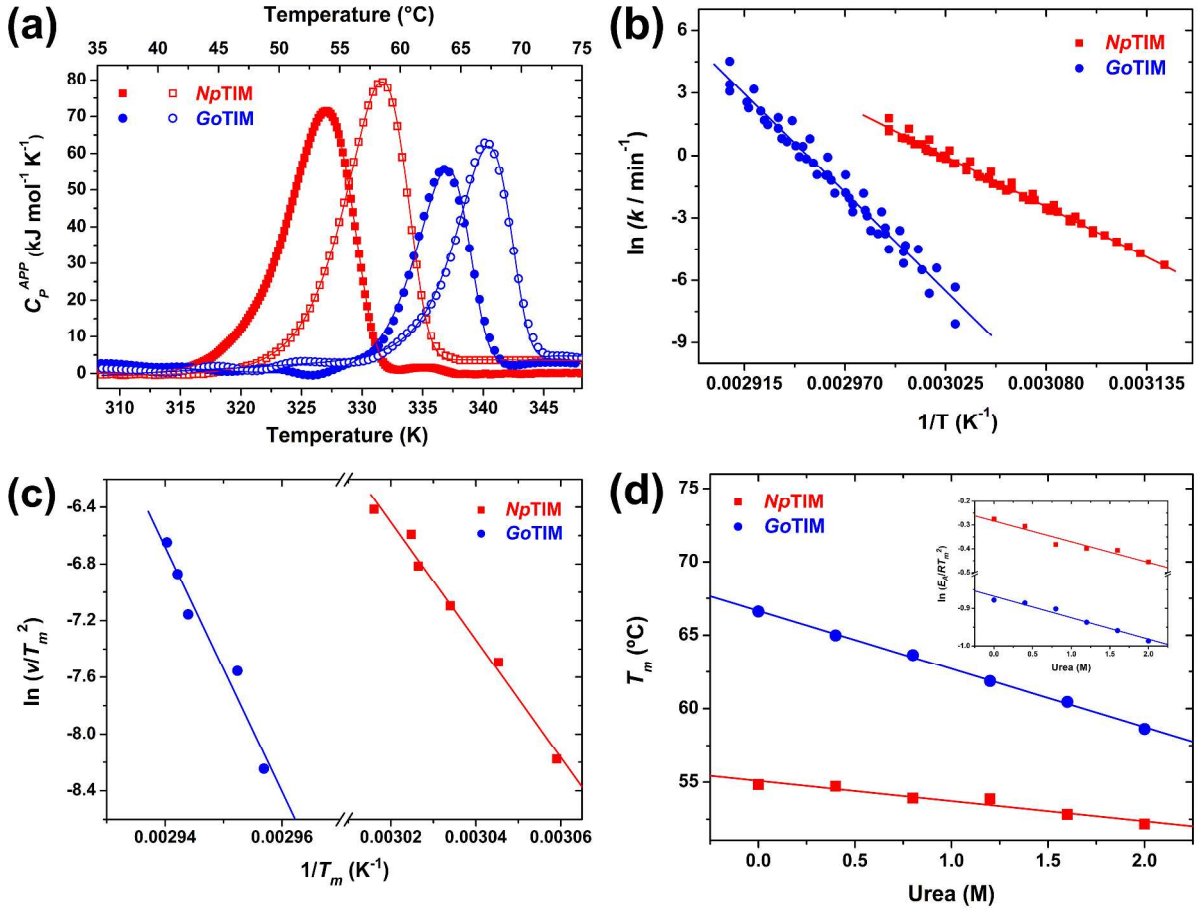

Fig. 2. Irreversible thermal unfolding of *Np*TIM and *Go*TIM. **(a)** DSC thermograms at 0.5 and 3.0 K min^{-1} (closed and open symbols, respectively). Lines show the best fit to the two-state irreversible model (eqns (3) and (4)). Other scan rates (1.0, 1.5, 2.0 and 2.5 K min^{-1}) were also assayed but are not shown for clarity. **(b)** Arrhenius plot from data obtained at six scan rates varying from 0.5 to 3.0 K min^{-1}.The lines are the best fit to the Arrhenius equation (eqn (2)). **(c)** Effect of scan rate on T_m for the unfolding of *Np*TIM and *Go*TIM. Lines represent the best fits to eqn (5). **(d)** Effect of urea concentration on the T_m. The slopes of the linear fits provide the value of dT_m/d[urea] used in eqn (6). The inset illustrates the calculation of the derivative dln(E_A/RT_m)/d[urea] that is also involved in the calculation of kinetic $m^{\ddagger}$ values. Protein concentration in all panels was 15 μM.

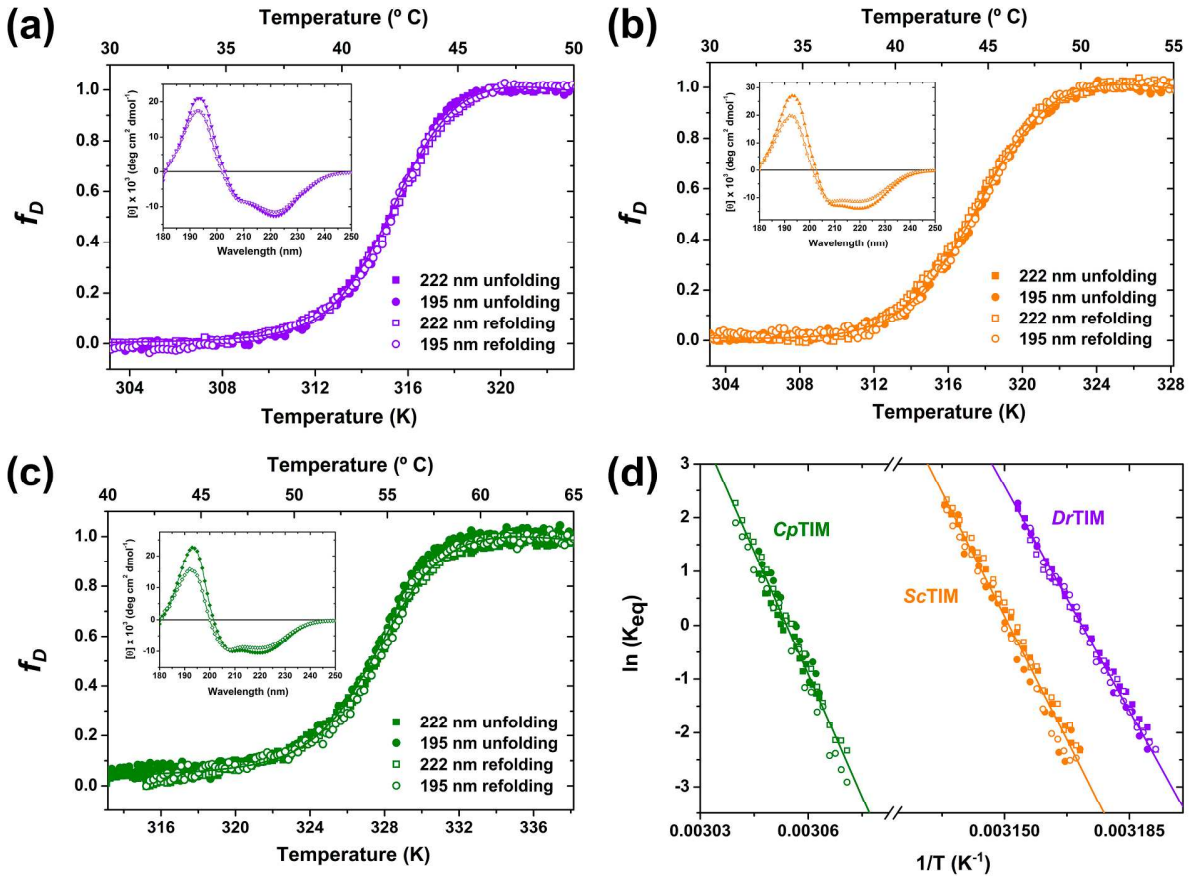

Fig. 3. Reversible thermal unfolding of *Dr*TIM, *Sc*TIM and *Cp*TIM followed by CD**.** Unfolding/refolding data (closed and open symbols, respectively) for *Dr*TIM **(a)**, *Sc*TIM **(b)**, and *Cp*TIM **(c)** were followed at 220 nm (squares) and 195 nm (circles) at 1.0 K min^{-1}. Lines show the best fit to a two-state dimer dissociation model ($N_2 \rightleftharpoons 2U$; eqn (7)). The inset shows the CD spectra of native TIM at 25 °C (closed symbols) and refolded TIM after a heating cycle (open symbols). **(d)** van't Hoff plots of unfolding and refolding data (closed and open symbols, respectively) followed at 220 nm (squares) and 195 nm (circles). Lines are the best fits to the eqn (7). ΔH_{vH} values derived from these fittings are reported in Table 2. In all panels, protein concentration was 15 μM.

thermal unfolding process. DSC traces showed an increase in melting temperature (T_m) with scan rate (Fig. 2a, and Fig. S4, ESI†) and no endotherm was observed in a second heating run, showing that *Np*TIM and *Go*TIM display kinetic control. The following evidences indicate that the temperature-induced unfolding of these proteins can be described by the two-state irreversible model: *(i)* at all scanning rates, the thermograms were well-fitted (Fig. 2a), giving similar Activation Energy (E_A) values (Table S1, ESI†), *(ii)* the Arrhenius plots were linear (Fig. 2b), and *(iii)* the data consistency test was successful, *i.e.* eqn (5) was fulfilled (Fig. 2c). These evidences also imply that the kinetically relevant transition state is dimeric. The average E_A obtained from the three methods are 360 ± 25 kJ mol^{-1} for *Np*TIM and 715 ± 46 kJ mol^{-1} for *Go*TIM (Table S1, ESI†). These values are similar to the lower and higher values reported for the E_A of EukTIMs (325-774 kJ mol^{-1}; Table S1, ESI†). A consequence of the E_A for *Go*TIM being twice that of *Np*TIM is that the denaturation rate at physiological conditions for *Go*TIM is many orders of magnitude slower than for *Np*TIM, indicating a much higher kinetic stability for the former. The fractional degree of exposure of the proteins to the solvent in the transition state ($m^{\ddagger}/m_{eq}$) was calculated from DSC experiments using different concentrations of urea (Fig. 2d). The values obtained for *Np*TIM and *Go*TIM (0.06 and 0.29 respectively) indicate that the transition state for thermal unfolding is native-like in both proteins (Table S1, ESI†).

2.3 The thermal unfolding of *Dr*TIM, *Sc*TIM and *Cp*TIM is a two-state equilibrium reversible process

For *Dr*TIM, *Sc*TIM and *Cp*TIM, the following experimental behaviour was found: *(i)* their CD spectra were very similar before and after a heating cycle (Fig. 3a-c inset) and unfolding and refolding transitions were super-imposable (Fig. 3a-c); the high temperature CD spectra of *Dr*TIM, *Sc*TIM and *Cp*TIM display the common spectral shape observed in thermally unfolded proteins with no residual structure, characterized by a broad shoulder around 220 nm and a large negative peak at ca. 200 nm (Fig. S5, ESI†);[10,65,66] *(ii)* T_m was independent of scan rate (Fig. S4, ESI†); *(iii)* DSC endotherms obtained in the first and second scans were almost identical (Fig. 4a-c) and *(iv)* catalytic activity of the refolded enzymes was between 84 and 96 % of the native samples. All these evidences show that the

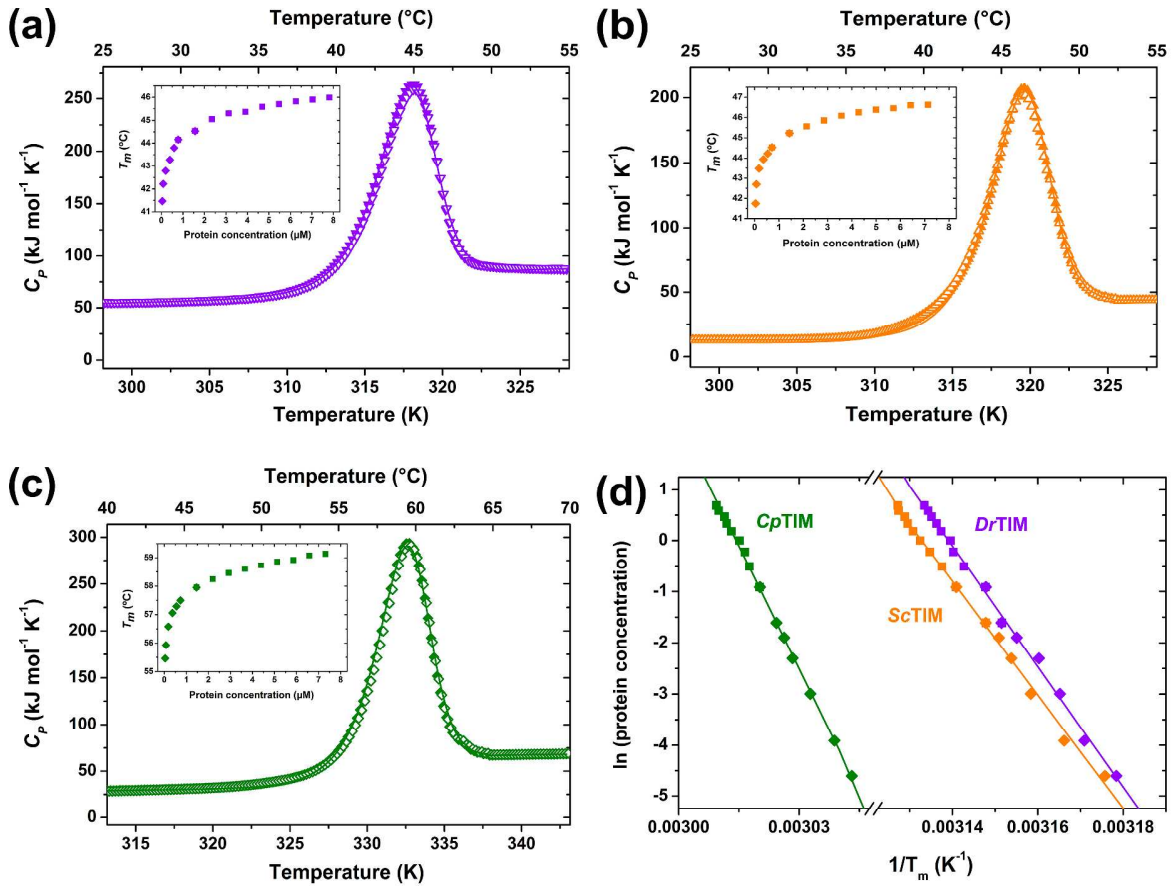

Fig. 4. Reversible thermal unfolding of *Dr*TIM, *Sc*TIM and *Cp*TIM followed by DSC. The first and second endotherms (closed and open symbols, respectively) are shown for *Dr*TIM **(a)**, *Sc*TIM **(b)**, and *Cp*TIM **(c)**. Continuous curves show the best fit to a two-state dimer dissociation model ($N_2 \rightleftharpoons 2U$; eqn (8)). In all panels, the scan rate was 1.5 K min^{-1} and protein concentration of 15 μM. The inset shows the T_m values obtained by CD (diamonds) and DSC (squares) as a function of TIM concentration at a scan rate of 1.5 K min^{-1}. **(d)** Takahashi-Sturtevant plot for CD and DSC data (diamonds and squares, respectively). The lines are the best fit to eqn (9).

temperature-induced unfolding of *Dr*TIM, *Sc*TIM and *Cp*TIM is reversible and at of the refolded enzymes was between 84 % and 96 % of the native samples. All these evidences show that the temperature-induced unfolding of *Dr*TIM, *Sc*TIM and *Cp*TIM is reversible and at equilibrium in the experimental conditions tested. All this contrasts with the thermal unfolding of *Np*TIM, *Go*TIM and all previously studied TIMs which is irreversible or presents hysteresis[36,38,43-53] and their high temperature CD spectra that show the shape and decrease in spectral signal observed in unfolded and aggregated proteins (Fig. S5, ESI†).

The thermal unfolding of *Dr*TIM, *Sc*TIM and *Cp*TIM can be well-described by a two state dissociation/unfolding process; the unfolding melts followed by CD (Fig. 3a-c), as well as the DSC traces (Fig. 4a-c) were well-fitted to this model. In addition, the enthalpy change from the native state to unfolded state (ΔH_{vH}) calculated from the van't Hoff analysis of CD data (Fig. 3d) and those obtained from DSC experiments were similar (Table 2). Likewise, T_m increased with protein concentration, as expected for the coupled dissociation/unfolding of a dimeric protein (Fig. 4a-c inset) and the Takahashi-Sturtevant plot constructed with CD and DSC data was linear (Fig. 4d). Finally, the ratio of the van´t Hoff and calorimetric enthalpies obtained (Table 2) were in excellent agreement with that expected (1.33) for a coupled dissociation/unfolding process.[67]

2.4 The global stability curve of *Dr*TIM, *Sc*TIM and *Cp*TIM

The reversibility and equilibrium conditions found in the temperature-induced unfolding of *Dr*TIM, *Sc*TIM and *Cp*TIM, allowed the estimation of ΔH, T_m and change in heat capacity of unfolding (ΔC_p) from DSC measurements (Tables 1 and 2). The ΔC_p was obtained from the DSC thermograms at different TIM concentrations. To this end, two different procedures were employed: *(i)* C_p for the native and unfolded state was calculated from the difference of absolute heat capacity in native and unfolded state (see Material and Methods) and *(ii)* DSC traces were fitted to an equation that includes ΔC_p as a fitting parameter (eqn (8)). The average ΔC_p obtained using these methods were 27.6 ± 1.7 for *Dr*TIM, 26.8 ± 2.5 for *Sc*TIM and 28.5 ± 2.1 kJ mol^{-1} for *Cp*TIM (Table 2). These values are in accordance with the ΔC_p predicted from the

Table 2. Thermodynamic parameters of reversible thermal unfolding of *Dr*TIM, *Sc*TIM and *Cp*TIM.

Physicochemical Parameter	*Dr* TIM	*Sc* TIM	*Cp* TIM
Enthalpy change (ΔH) (kJ mol^{-1})			
ΔH_{vH} by DC	1071 ± 29	1178 ± 38	1205 ± 46
ΔH_{vH} by DSC	1121 ± 42	1255 ± 96	1230 ± 67
ΔH_{cal} by DSC	811 ± 34	941 ± 33	895 ± 50
Calorimetric criterion[a] ($\Delta H_{vH}/\Delta H_{cal}$)	1.38 ± 0.06	1.33 ± 0.09	1.37 ± 0.08
$\Delta H'$ from a Takahashi-Sturtevant plot	1108 ± 46	1150 ± 33	1247 ± 63
Heat capacity change (ΔC_p) (kJ mol^{-1} K^{-1})			
Experimental ΔC_p	27.6 ± 0.9	25.9 ± 3.4	28.5 ± 3.4
Fitted ΔC_p[b]	27.2 ± 0.9	27.6 ± 1.7	28.5 ± 1.7
Average ΔC_p	27.6 ± 1.7	26.8 ± 2.5	28.5 ± 2.1
Predicted ΔC_p based on amino acidic sequence			
ΔC_p by ref. 68	32.2	35.6	35.2
ΔC_p by ref. 69	28.9	30.1	29.3
Predicted ΔC_p based on ΔASA correlations			
ΔC_p by ref. 70	57.8	57.8	59.4
ΔC_p by ref. 71	43.9	43.9	45.2
ΔC_p by ref. 72	71.1	71.1	73.2
ΔC_p by ref. 73	40.2	40.2	41.8
ΔC_p by ref. 69	33.1	33.1	35.2
ΔC_p by ref. 74	37.1	38.1	40.2

[a] Errors are the standard deviation of different experiments at different protein concentration and/or scan rate.

[b] Calculated with DSC values.

[c] ΔC_p obtained from DSC experiments fitted to eqn (8).

number of amino acids of these TIMs;[69] they are, however, much lower than the ΔC_p predicted from other parameterizations, as previously reported for other dimeric systems.[11]

Using eqn (10), the global stability curves, *i.e.* $\Delta G(T)$ for the coupled dissociation/unfolding (ΔG_{tot}) as a function of temperature, were calculated and are shown in Fig. 5. ΔG_{tot} values near the T_m, obtained from CD experiments (solid symbols in Fig. 5) are in excellent agreement with the stability curve generated using DSC data. ΔG_{diss} values obtained from dilution experiments carried out at different temperatures are also shown (open symbols in Fig. 5). *D. radiodurans*, *S. coelicolor* and *C. perfringens* are mesophiles, however, when the stability curves of their TIMs are compared, a 14 degrees difference in T_m and a 17 kJ mol^{-1} difference in ΔG_{tot} was found. Changes in T_S (the temperature where $\Delta S = 0$), ΔH_{TS} (enthalpy change at T_S), and/or ΔC_p modulate the shape of the stability curve.[75] In the present case, these differences are mainly due to changes in ΔH_{TS} and T_S (Fig. 5). ΔH_{TS} can be changed by mutation and has been related to an increase in stabilizing interactions in the native state; T_S was originally not

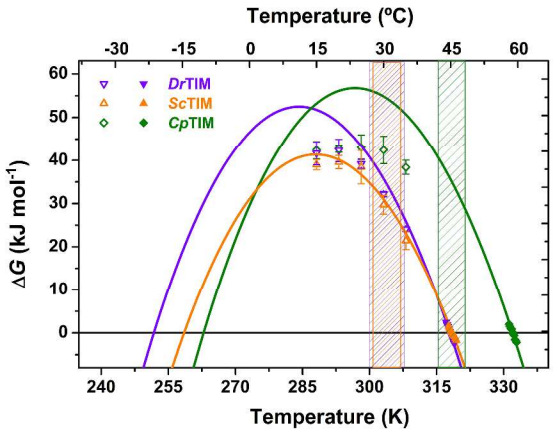

Fig. 5. Stability curves of *Dr*TIM, *Sc*TIM and *Cp*TIM. Solid lines are the stability curves constructed with data obtained by DSC and the Gibbs-Helmholtz equation (eqn (10)) (Data used: *Dr*TIM (purple): ΔH = 811 kJ mol^{-1}, ΔC_p = 27.6 kJ mol^{-1} K^{-1} and T_m = 317.4 K; *Sc*TIM (orange): ΔH = 941 kJ mol^{-1}, ΔC_p = 26.8 kJ mol^{-1} K^{-1} and T_m = 318.5 K; *Cp*TIM (green): ΔH = 895 kJ mol^{-1}, ΔC_p = 28.5 kJ mol^{-1} K^{-1} and T_m = 331 K). Open symbols indicate experimental ΔG values obtained by CD in the transition (Fig. 3a-c) and closed symbols show the dissociation ΔG obtained from dilution experiments (Fig. 1) carried out at different temperatures (288.15 to 308.15 K). Purple, orange and green stripes are the temperature ranges of optimal growth (TOG) of *D. radiodurans*, *S. coelicolor* and *C. perfringens*, respectively.[77-79]

considered a source of stabilization, however, recently it has been reported that changes in both ΔH_{TS} and T_S can increase T_m.[76] A comparison of the temperature range of optimal growth (TOG)[77-79] in relation to the stability curve indicates that these proteins function at temperatures higher than their maximal stability (Purple, orange and green stripes in Fig. 5). It is interesting to note that an increase in T_m is accompanied by an increase in TOG, in such a way that conformational stability within the TOG fluctuates in a narrow range (24.3 to 39.8 kJ mol^{-1}).

2.5 Three-dimensional structure of BacTIMs

In order to correlate the thermodynamic and structural properties of BacTIMs, crystallization assays were performed with all of them. Good quality crystals were obtained for *Go*TIM, *Dr*TIM, *Sc*TIM and *Cp*TIM, and their structure was therefore solved at high/medium resolution by X-ray crystallography. Data collection and refinement statistics are shown in Table S2, ESI†. Crystallographic data show a dimeric association state, in agreement with SEC experiments (Table 1). The canonical $(\beta\alpha)_8$ topology of the barrel is very similar in all the structure of the BacTIMs determined in this work (Fig. 6a). The orientation of the monomers with respect to each other in the dimer is also similar; in fact, it is fairly conserved among TIMs from the three domains of life. The so-called "catalytic side" of TIM barrels is formed by eight loops that connect the carboxyl-terminal end of the β-strands with the amino-terminal end of the α-helix. In BacTIMs, as well as in all previously reported TIM structures, these loops provide the catalytic residues and most of the interactions that stabilize the

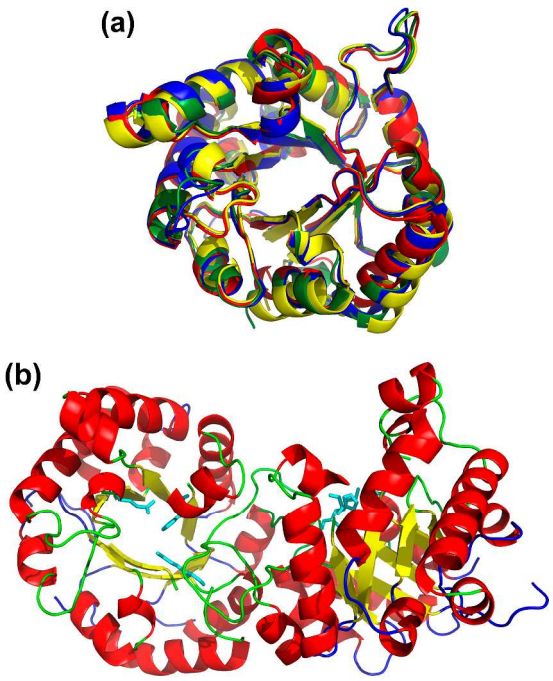

Fig. 6. The three-dimensional structure of TIM. **(a)** Structural superposition of the monomer of *Go*TIM (red), *Dr*TIM (yellow), *Sc*TIM (green), and *Cp*TIM (blue). **(b)** Ribbon representation of the 3D structure of the *Cp*TIM dimer. Loops from the *catalytic side* are shown in green whereas *stability loops* are shown in blue. Catalytic residues are shown in cyan sticks.

monomer-monomer interface. The other side of the barrel is formed by the "stability loops" that connect the carboxyl-terminal end of the α-helices with the amino-terminal end of the β-strands (Fig. 6b). The correlation between structure and thermodynamics will be discussed below in the context of the reversibility in the folding process.

2.6 On the possible relation between molecular properties and reversibility

The molecular origin of the reversibility of protein folding is not known. Hence, as a first step to advance towards that knowledge, it is interesting to establish reasonably supported relations between reversibility and the molecular level properties of the protein. Here, we explored such possible relations at three levels: *(i)* Sequence-related properties and their phylogenetic relations, *(ii)* the structural properties of the stable states, and *(iii)* the physicochemical properties of the unfolding/refolding transition between them. To this end, the three reversible TIMs reported in this work, herein named "RevTIMs", were compared with the 19 dimeric TIMs that show irreversible thermal unfolding, henceforth called "IrrevTIMs". Note that for three IrrevTIMs there is no structure available.

(i) Sequence-related properties and phylogenetic relations. The identity among the sequence of the three RevTIMs is between 40% and 52%. The sequence identity among the three

Table 3. Isoelectric point, cavity volume and melting temperature for IrrevTIMs and RevTIMs.

	TIM	pI[a]	Cavity volume (Å^3)[b]	T_m(°C)[c]	Reference[d]
IrrevTIMs	*Eh* TIM[e]	6.1	3777	40.5 / 56.3	51
	Mm TIM	4.8	3927	41.0	44
	Ec TIM	5.6	4667	54.0	44
	Mt TIM	5.9	3087	55.0	49
	Np TIM	5.0	ND	55.2	This work
	Tb TIM	9.1	3780	55.8	52
	Oc TIM	7.1	3485	56.0	43
	Gl TIM	7.1	3920	57.5	50
	Yt TIM	5.8	3699	59.1	47
	Tc TIM	8.6	3414	59.2	52
	Ts TIM	6.6	ND	62.3	48
	Lm TIM	8.2	3531	62.5	52
	Hs TIM	6.5	3259	63.1	53
	Ss TIM	7.1	ND	63.9	48
	Pf TIM	6.1	4452	65.0	46
	Go TIM	6.3	4010	65.6	This work
	Tv TIM[f]	5.6	3383	67.1	38
	Gg TIM	6.7	3518	67.2	36
	Gs TIM	5.2	2503	76.0	45
	Mean (μ)	6.5	3651	59.3	
	Standard deviation (σ)	1.2	514	8.5	
	$\mu + \sigma$	7.7	4165	67.8	
	$\mu - \sigma$	5.3	3137	50.7	
RevTIMs	*Dr* TIM	4.9	2134	44.6	This work
	Sc TIM	5.2	2921	45.3	This work
	Cp TIM	5.0	2241	58.3	This work

[a] Determined by ProtParam software.[80]

[b] Cavity volume in the native state was calculated without water molecules as described in Materials and Methods.

[c] Value reported in experiments at pH 7.4 with protein concentration of ≈10-15 μM and scan rate of 1.0 K min^{-1}, except for *Tv*TIM in which the scan rate used was 2.0 K min^{-1}.

[d] T_m values were obtained from these references.

[e] The values reported correspond to dimer dissociation and monomer unfolding.

[f] Reported T_m of the dimeric Ile45 variant.

Abbreviations: *Cp*TIM, TIM from *Clostridium perfringens*; *Dr*TIM, TIM from *Deinococcus radiodurans*; *Ec*TIM, TIM from *Escherichia coli*; *Eh*TIM, TIM from *Entamoeba histolytica*; *Gg*TIM, TIM from *Gallus*; *Go*TIM, TIM from *Gemmata obscuriglobus*; *Gl*TIM, TIM from *Giardia lamblia*; *Gs*TIM, TIM from *Bacillus stearothermophilus;* *Hs*TIM, TIM from *Homo sapiens*; *Lm*TIM, TIM from *Leishmania mexicana*; *Mm*TIM, TIM from *Moritella marina*; *Mt*TIM, TIM from *Mycobacterium tuberculosis*; *Np*TIM, TIM from *Nostoc punctiforme*; *Oc*TIM, TIM from *Oryctolagus cuniculus*; *Pf*TIM, TIM from *Plasmodium falciparum*; *Sc*TIM, TIM from *Streptomyces coelicolor*; *Ss*TIM, TIM from *Sus scrofa*; *Tb*TIM, TIM from *Trypanosoma brucei*; *Tc*TIM, TIM from *Trypanosoma cruzi*; *Ts*TIM, TIM from *Taenia solium*; *Tv*TIM, TIM from *Trichomonas vaginalis*; *Yt*TIM, TIM from *Saccharomyces cerevisiae*.

Table 4. Structural features used for comparison between IrrevTIMs and RevTIMs.

Structural property	*Dr* TIM	*Sc* TIM	*Cp* TIM	Average RevTIMs	Average IrrevTIMs
Total ASA of the folded oligomer (Å^2)	18107	19475	19947	19176 ± 780	19040 ± 629
Hydrophobic ASA of the folded oligomer (Å^2)	10389	11367	11481	11079 ± 490	11498 ± 600
% Hydrophobicity[a]	57.4	58.4	57.6	57.8 ± 0.4	60.4 ± 1.3
Total ΔASA buried on folding of the monomer (Å^2)	25222	26550	26679	26151 ± 658	27056 ± 740
Hydrophobic ΔASA buried on folding of the monomer (Å^2)	18367	19465	19269	19034 ± 478	19552 ± 375
% Hydrophobicity[b]	72.8	73.3	72.2	72.8 ± 0.5	72.3 ± 1.9
Total ΔASA of the folded monomer buried on assembly (Å^2)	3113	3425	3467	3335 ± 158	3275 ± 207
Hydrophobic ΔASA of the folded monomer buried on assembly (Å^2)	2131	2286	2339	2252 ± 89	2005 ± 354
% Hydrophobicity[c]	68.5	66.7	67.5	67.6 ± 0.7	61.2 ± 2.8
Total ΔASA of the unfolded monomer on assembly (Å^2)	53558	53524	56826	55636 ± 1474	57388 ± 1365
Hydrophobic ΔASA of the unfolded monomer on assembly (Å^2)	38864	41217	40878	40320 ± 1038	41110 ± 835
% Hydrophobicity[d]	72.6	77.0	71.9	73.8 ± 2.3	71.6 ± 2.1
ΔASA_{dissoc} / ΔASA_{tot} (%)	5.8	6.4	6.1	6.1 ± 0.3	5.7 ± 0.4
$\Delta ASA_{dissoc\ hydrophob}$ / $\Delta ASA_{tot\ hydrophob}$ (%)	5.5	5.5	5.7	5.6 ± 0.1	4.8 ± 0.7
Molecular volume of the oligomer (Å^3)	62052	67188	69885	66375 ± 3249	67339 ± 2221
Number of cavities in oligomer (without solvent)	10	11	9	10 ± 1	16 ± 3
Total volume of cavities in oligomer (Å^3) (without solvent)	2134	2921	2241	2432 ± 349	3651 ± 498
Total volume of the biggest cavity in the oligomer (Å^3)	324	683	290	432 ± 178	1001 ± 209
Total volume of cavities in oligomer (Å^3) (with solvent)	928	1335	1008	1090 ± 176	1908 ± 366

[a] Errors are the standard deviation from averaged values of all structures in each group.

[b] % Hydrophobicity = (hydrophobic ASA of the oligomer / total ASA of the oligomer) * 100%.

[c] % Hydrophobicity = (hydrophobic ΔASA buried on folding of the monomer / total ΔASA buried on folding of the monomer) * 100%.

[d] % Hydrophobicity = (hydrophobic ΔASA of the folded monomer buried on assembly / total ΔASA of the folded monomer buried on assembly) * 100%.

[e] % Hydrophobicity = (hydrophobic ΔASA of the unfolded monomer on assembly / total ΔASA of the unfolded monomer on assembly) * 100%.

RevTIMs is similar to those between RevTIMs and IrrevTIMs (Table S3, ESI†). There are no significant differences on the abundance of a particular group of amino acids between both groups (Table S4, ESI†). There is also no particular region in the sequence that is different amongst RevTIMs and IrrevTIMs (Fig. S6, ESI†). Regarding the global properties of the sequence, RevTIMs tend to have a lower pI than IrrevTIMs (Table 3); in accordance with this, it is known that reversibility increases when the experimental pH is far away from the pI of the protein.[81-83] It should be noted, however, that some IrrevTIMs such as TIM from *Moritella marina* (*Mm*TIM), *Np*TIM and TIM from *Geobacillus stearothermophilus* (*Gs*TIM) show a pI similar to that of RevTIMs. Nevertheless, the three RevTIMs present pI values outside the $\mu \pm \sigma$ range determined for the IrrevTIMs (Table 3). Concerning the phylogenetic relation between the species where RevTIMs come from, *S. coelicolor* and *C. perfringens* belong to the Actinobacteria and Firmicutes, respectively. Both phyla form the Posibacteria group, whereas *D. radiodurans* belongs to the Deinococcus-Thermus phylum that forms part of the distant Eobacteria group (Fig. S1, ESI†). Therefore reversibility does not seem to be restricted to a particular phylogenetic group.

(ii) Structural properties of stable states. The properties of the unfolded state may be involved in reversibility. *Np*TIM and *Go*TIM, the two IrrevTIMs reported here, show the spectra observed when thermal unfolding is associated to irreversible aggregation and is consequently not suitable for an estimation of residual structure; *Yt*TIM, which presents in some conditions a reversible thermal unfolding transition with a marked hysteresis, shows a high temperature CD spectra with evidence of residual structure.[47] In contrast, the CD spectra of the thermally-induced unfolded states of RevTIMs do not show evidence of secondary structure (Fig. S5, ESI†). Therefore, it is possible that the absence of residual structure may be related to reversibility. There are no significant differences in the backbone trace of the native state of RevTIMs and IrrevTIMs (Fig. 6a). The length of secondary structure elements and the conformation of loops are very similar (Table S5, ESI†), and the average RMSD values among RevTIMs and IrrevTIMs are also indistinguishable (0.2-1.5 Å; Table S3, ESI†). It should be

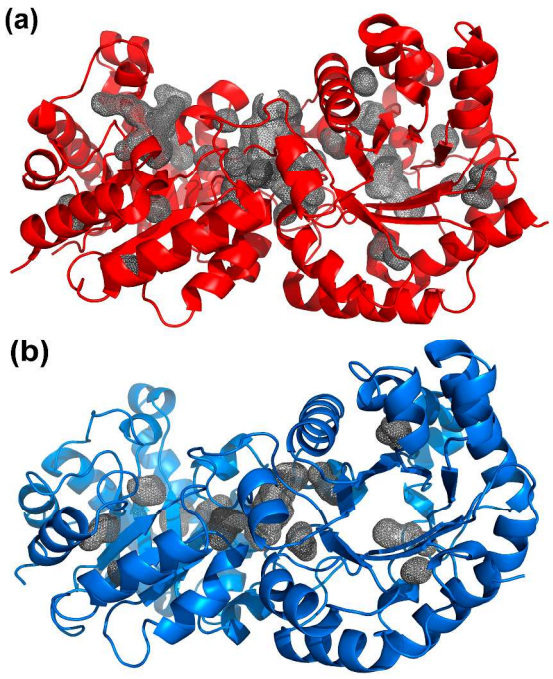

Fig. 7. Internal cavities in the three-dimensional structure of TIM. The structure and cavities are shown for: **(a)** *Go*TIM, an example of an IrrevTIM, and **(b)** *Cp*TIM, an example of a RevTIM. Total volume of cavities in oligomer of *Go*TIM and *Cp*TIM are 4010 Å^3 and 2241 Å^3, respectively.

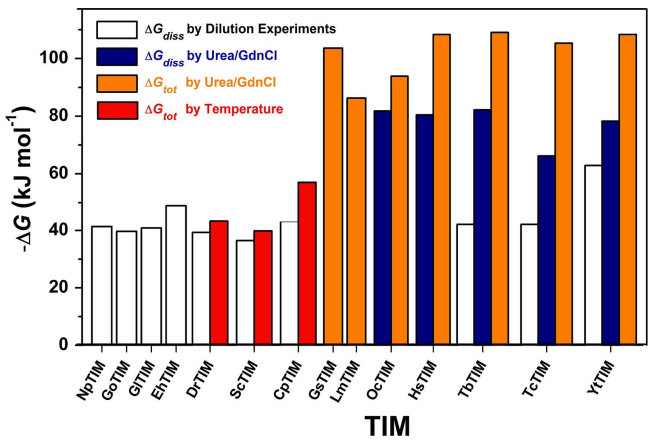

Fig. 8. Comparison of the reported free energies for different TIMs. Red and orange bars indicate ΔG_{tot} at 25 ºC, blue bars are ΔG_{diss} at 25 ºC and white bars represent ΔG_{diss} values derived from dilution experiments previously reported[56-60] and determined in this work. Data for *Hs*TIM, *Gs*TIM, *Oc*TIM, *Lm*TIM and *Yt*TIM were obtained from urea or guanidinium hydrochloride experiments,[23-37] whereas data for *Dr*TIM, *Sc*TIM and *Cp*TIM are from the DSC experiments in this work.

emphasized that, the four structures determined in this work, as well as most of the fifteen structures used for comparison, were crystallized without ligand; consequently, most of them show the catalytic loop 6 in the "open" conformation (Table S6, ESI†). Regarding the structural features of the monomers, no differences were found when the interactions within the monomer were compared (Table S5, ESI†). Likewise, when the dimer interface of RevTIMs and IrrevTIMs was compared, no differences in the number of hydrogen bonds or salt bridges between the monomers were found (Table S5, ESI†). The total surface buried upon association and its hydrophobic content were also similar (Table 4).

The only structural difference between the native state of RevTIMs and IrrevTIMs so far detected relates to cavities. RevTIMs show a lower number of cavities; their volume is approximately 40 % lower than that of IrrevTIMs (Table 3 and 4). The native structure of the three RevTIMs have cavity volumes values outside the $\mu \pm \sigma$ interval determined for the IrrevTIMs (Table 3). The size of the biggest cavity, located at the interface between β-strands 5-7 and α-helices 5-6 (comprising residues 90-120, 145-160 and 195-200; Fig. S6, ESI†), is the main responsible of the cavity volume difference between RevTIMs and IrrevTIMs (Table 4 and Fig. 7). There are no previous reports on the relation between cavity volume in the native state and reversibility in unfolding transitions; however, it has been suggested that internal cavity volume influences the stability and the unfolding kinetics of proteins.[75,84,85]

(iii) Physicochemical properties of the unfolding/refolding transition. It is more likely to find reversible thermal unfolding in proteins that exhibit a low T_m because high temperatures promote the chemical modification of amino acid side chains. In agreement, *Dr*TIM and *Sc*TIM present some of the lower T_ms reported to date. It is worth noting that, however, the T_m of *Cp*TIM is higher than eight TIMs that show irreversible thermal unfolding (Table 3). In fact, *Cp*TIM is the only RevTIM whose T_m is within the $\mu \pm \sigma$ interval determined for IrrevTIMs (Table 3). Regarding thermodynamic stability, ΔG_{diss} obtained from dilution experiments is very similar in both RevTIMs and IrrevTIMs (white bars in Fig. 8), and this suggests that the stability of the interface does not correlate with reversibility. Concerning the overall stability of the dimer, ΔG_{tot} for IrrevTIMs is higher than the ΔG_{tot} values of RevTIMs (compare orange and red bars in Fig. 8) and consequently, it is possible that reversibility is related to a lower ΔG_{tot}. It should be noted, however, that ΔG_{tot} for IrrevTIMs was obtained from chemical unfolding experiments whereas ΔG_{tot} for the reversible ones was obtained using temperature as a perturbant. Despite this, it is reasonable to consider a correlation between reversibility and low conformation stability.

The equilibrium thermal unfolding of all RevTIMs can be well described with a two state model (Fig. 3a-c and 4a-c), and most of the studied IrrevTIMs show a single cooperative transition described by a single T_m value (Table 3); hence, it seems that there are no stable and/or populated equilibrium intermediates involved. Nevertheless, it is likely that the aggregation properties of transient intermediates play a role in determining the reversibility of folding transitions. In this regard, the monomeric intermediate observed in the thermal unfolding of *Eh*TIM unfolds irreversibly.[51] Likewise, evidence

for kinetic intermediates was found in the highly irreversible temperature-induced unfolding of *Tc*TIM.[86] Consequently, it is worthwhile to explore a possible relation between two state unfolding and reversibility**.** At 25°C, *Dr*TIM and *Sc*TIM show that $\Delta G_{tot} \approx \Delta G_{diss}$ whereas for *Cp*TIM ΔG_{diss} is ≈ 75% of ΔG_{tot} (compare white and red bars in Fig. 8). ΔG_{tot} from temperature-induced unfolding experiments has not been obtained previously for IrrevTIMs; however when ΔG_{tot} has been obtained using urea or GndHCl as perturbants, ΔG_{diss} was also found to be a major component of ΔG_{tot} (compare blue and orange bars in Fig. 8). It is worth stressing that in previous reports,[56-60] reversibility has not been tested in the dilution experiments used to obtain ΔG_{diss}. This, and the different nature of chemical unfolding and dilution, may explain why these values are not always similar to ΔG_{diss} obtained from urea and GndHCl-induced unfolding experiments (compare white and blue bars in Fig. 8). However, it seems that irrespectively of the perturbant, the dissociation event is the main component of the conformational stability of TIM.[24-38]

There are two extreme scenarios for a dissociation process; in the rigid body case, subunit dissociation takes place without the unfolding of the monomers; on the other extreme, dissociation is coupled to complete monomer unfolding (two state behaviour). Reversibility is likely related to the cooperativity of the folding process. For example, if TIM monomers were isolated from the native dimer in a rigid body scenario, each of them would expose a surface area of 1645 Å^2 (Table 4), nearly 70 % of this area is hydrophobic, increasing the chances of aggregation; therefore, the presence of stable monomeric intermediates would likely reduce reversibility. Analysis of the structural data for TIM from several species shows that the association of the monomers to form the native dimer accounts for ≈ 5-6 % of the overall ΔASA calculated in going from the unfolded monomers to the folded dimer (Table 4). From structure-based parameterizations, we estimate that for the rigid body case, dissociation would contribute a similar 5-6 % of the total ΔC_p (Table 2). In contrast, the available experimental data on the chaotrope-induced three state unfolding of TIM from several organisms show that the dissociation step accounts for ≈ 75 % of the overall conformational stability of the dimer.[32] Likewise, dissociation represents 55 % of the total enthalpy change; this has led to the conclusion that dimer dissociation leads to extensive unfolding of the monomers, *i.e.* dissociation is not a rigid body process.[51] In accordance, folding and association are strongly coupled in thermally unfolded *Yt*TIM.[47] *Dr*TIM, *Sc*TIM and *Cp*TIM show the extreme cooperative behaviour, that is, their thermal unfolding is a two state equilibrium process where isolated monomers are not stable at all. In agreement, ΔG_{diss} and ΔG_{tot} are similar for these proteins (Fig. 5 and 8). It is then tempting to correlate reversibility with two state behaviour. Nevertheless, it should be pointed out that the temperature-induced unfolding of many IrrevTIMs shows a single transition; therefore, extreme cooperativity does not by itself determine reversibility.

From the above discussion about the possible correlations between reversibility and the molecular level properties of TIM, it appears that there is a delicate balance between several contributions whose concerted interplay is necessary to achieve thermal reversibility in oligomeric enzymes. All the correlations between molecular level properties and reversibility proposed in this work were obtained from the analysis of the stability and structure of a limited number of proteins. Clearly, more quantitative data, such as the physicochemical characterization of TIMs from yet unexplored branches of the tree of life, are needed to further assess the findings in this work. A clear avenue to obtain a more detailed atomic description of the unfolding and dissociation of TIM is the use of Molecular Dynamics. This methodology is a valuable tool to evaluate intermolecular interactions at the finest level of detail.[87] Steered molecular dynamics have been successfully used for the estimation of protein-ligand[88] and protein-protein energetics;[89] the optimization of this and other methodologies for the analysis of protein-protein interactions is a current focus of research.[90] It is likely that the Molecular Dynamics approach, applied to the *in silico* unfolding of RevTIMs and IrrevTIMs, will be able to dissect the location of conformational changes taking place upon dimer dissociation and monomer unfolding, as well as the role of their coupling in reversibility. In addition, the kinetic characterization of the thermal unfolding of RevTIMs should bring more information regarding the unfolding pathway followed by these proteins.

3. Conclusions

The results presented in this work show that the thermal unfolding of a given protein architecture, such as the TIM barrel, can exhibit kinetic or thermodynamic control. *Np*TIM and *Go*TIM show kinetic control and their unfolding activation energies are in the low and high range of those determined for EukTIMs. It has been suggested that kinetic stability is more strongly selected by evolution than thermodynamic stability because the former facilitates irreversible alteration processes even when a high thermodynamic stability is maintained.[91] Notably, *Dr*TIM, *Sc*TIM and *Cp*TIM presented thermodynamic control and reversible thermal unfolding. Stability and reversibility are biotechnologically relevant;[92,93] however, the reasons underlying the reversibility of the unfolding process are not understood. In this work we found no correlation between this behaviour and the composition or the gross structural properties of TIM; however, low pI, the absence of residual structure in the unfolded state, a small cavity volume in the native state, low conformational stability and low T_m, may be involved. It is very possible that reversibility is encoded in the folding pathway. In this respect, one of the main conclusions derived from the characterization of the folding mechanism of monomeric TIM barrels is the presence of intermediates that have been related to the folding of particular β/α modules within the barrel. In contrast, the dimeric TIM barrels studied in this work show two state thermal unfolding. It is therefore possible that extreme cooperativity and reversibility are related.

For all living organisms from bacteria to mammals, temperature is probably the most common and natural stress

agent at the molecular level. In fact, life at "constant temperature" is a recent evolutionary event.[94,95] Molecular mechanisms such as the chaperonin system have evolved to help the cells to deal with temperature stress.[96-98] TIM has not been identified as a GroEL substrate, albeit TIM barrels are common substrates of the chaperonin system in *E. coli*.[99] Because oligomeric TIM barrels are frequent in cells, reversibility in their folding/unfolding process is an evolutive advantage because it reduces the chance of non-productive irreversible aggregation and the load of the cellular chaperonin machinery. That such a common topological ensamble can unfold and refold without the help of the cellular machinery is indeed biologically relevant. Furthermore, the finding that the three reversible proteins come from organisms from different phyla suggests that reversibility in thermal unfolding may be more common than what is currently known.

4. Material and methods

4.1 Enzymes and biochemicals

α-Glycerol-phosphate dehydrogenase (GDH) was purchased from Roche. All other reagents were of analytical grade from Sigma-Aldrich. The water used was distilled and deionized.

4.2 Species and sequences selection

From the phylogenetic tree published by Cicarelli and cols[100] and the phylogenetic classification proposal by Cavalier-Smith,[54] we selected six representative species with evolutionary significance and biomedical or biotechnological importance belonging to six different phyla (different bacteria paraphyletic supertaxa; Fig. S1, ESI†): *Deinococcus radiodurans* (*Dr*TIM; phylum: Deinococcus-Thermus), *Nostoc punctiforme* (*Np*TIM; phylum: Cyanobacteria), *Gemmata obscuriglobus* (*Go*TIM; phylum: Planctomycetes), *Azotobacter vinelandii* (*Av*TIM; phylum: Proteobacteria), *Clostridium perfringens* (*Cp*TIM; phylum: Firmicutes), and *Streptomyces coelicolor* (*Sc*TIM; phylum: Actinobacteria). TIM sequences of these species were extracted from GenBank[6] and annotated with their identification number: *Dr*TIM (GI: 653293168), *Np*TIM (GI: 186684444), *Go*TIM (GI: 497733394), *Av*TIM (GI: 226946590), *Cp*TIM (GI: 18310284), and *Sc*TIM (GI: 490074698).

4.3 Cloning, expression, and purification of BacTIMs

The nucleotide sequence of the genes coding for BacTIMs were optimized for their expression in *E. coli*, synthetized and cloned in the pBluescript-II-SK(-) plasmid (Agilent Technologies) by Epoch Life Science (Missouri City, TX-USA). BacTIM genes were subcloned into the pET28b(+) vector (Novagen) using the terminal restriction sites for *Nde*I and *Xho*I. The genes were expressed in *E. coli* strain BL21(DE3)p*Lys*S (Invitrogen) transformed with the BacTIM-pET28b(+) plasmids. To this end, 1 L of Luria broth (LB) medium supplemented with 30 mg mL^{-1} kanamycin was inoculated with a 1 mL preculture and incubated at 37 ºC and 250 rpm. After an OD_{600} of 0.6-0.8 was reached, overexpression was induced by adding 0.8 mM IPTG; growth was continued by 16 hours. After incubation, cells were harvested by centrifugation (Thermo/SLA-3000, 15 min, 8000 rpm, 4 ºC), suspended in buffer A (35 mM NaH_2PO_4, 300 mM NaCl and 5 mM Imidazole, pH 8.0), lysed by sonication (Cole Parmer Ultrasonic Processor, 10 cycles in 45 s intervals, 30% pulse, 0 ºC) and centrifuged again (Sorvall/SS-34, 20 min, 13000 rpm, 4 ºC). Affinity chromatography was then performed using a Waters AP-2 column containing 30 mL of Protino-NiTED resin (Machererl-Nagel), coupled to an Akta system (GE Healthcare). The supernatant was loaded into the column previously equilibrated with buffer A and the nonbound fraction was washed with 110 mL of buffer A. Bound protein was eluted with a linear gradient of 5-500 mM Imidazole. BacTIM-containing fractions were pooled and dialyzed against 50 mM tris (hydroxymethyl) aminomethane (TRIS), 10 mM $CaCl_2$ (pH 8.0). His-tag was removed with the Thrombin CleanCleave kit (Sigma-Aldrich) using the manufacture´s protocol. Cleaved and not cleaved protein were separated by a second affinity chromatography step. Unbound fractions were pooled, dialyzed against buffer B (10 mM triethanolamine (TEA), 1 mM ethylenediaminetetraacetate (EDTA), and 1 mM dithiothreitol (DTT), pH 8.0), and finally purified using a MonoQ column HR 10/10 (GE Healthcare). The sample was eluted with a linear gradient of 0-500 mM NaCl in buffer B. BacTIMs, 99 % pure according to SDS-PAGE (12.5 % acrylamide), were stored at 4 °C until use. After His-tag removal, ≈ 35 milligrams of protein were obtained per liter of culture. We were unable to express *Av*TIM in pET28b(+). Although several vectors were assayed, expression was only observed in pET22a. Irrespectively of the expression conditions, the protein was always found in inclusion bodies, numerous refolding protocols were assayed without success. Interestingly, of the six sequences studied in this work, the *Av*TIM sequence was the only predicted by the Stability Index as an unstable protein.[101] Some measurements were carried out in 10 mM phosphate pH 8.0 (buffer C). Protein concentration, estimated from the absorbance at 280 nm (and the absorption coefficient calculated from the amino acid sequence) or using the Bicinchoninic acid assay, gave similar results.

4.4 Activity assays

Catalytic activity in the GAP to DHAP direction was determined by a coupled assay with GDH.[51] The reaction cell contained 1 mL of buffer D (100 mM TEA, 10 mM EDTA and 1 mM DTT, pH 8.0) with 2 mM GAP (except when catalytic constants were determined), 20 µg of GDH, and 0.2 mM NADH. Catalytic assays started with 0.27 nM BacTIM. NADH absorbance changes at 340 nm were followed in a Beckman DU7500 spectrophotometer at 25 ºC. For the determination of catalytic constants, the concentration of GAP ranged between 0.1 and 3 mM. Changes in NADH absorbance were linear with time, indicating that no dimer dissociation took place during activity assays.

4.5 Hydrodynamic measurements

Size-exclusion-chromatography experiments were performed on a Superdex 75 HR 10/30 column, equilibrated with buffer B, coupled to an Akta System (GE Healthcare). The elution volume was independent on protein concentration in the tested range (0.4-20 μM). Stokes-radii were calculated from elution volumes and a calibration curve constructed using six different proteins (albumin, ovoalbumin, carbonic anhydrase, lysozyme, ribonuclease and cytochrome C).[102]

4.6 Stability to dilution experiments

The stability of the dimer was estimated from dilution experiments. BacTIMs were incubated for 24 hours at several temperatures (15 to 35 °C) and different concentrations (0.4 nM to 18 μM) in buffer D. Subsequently activity was determined at the incubation temperature with 0.27 nM BacTIM. For reversibility tests 1.5 L of 2 nM BacTIM were incubated at 25 °C for 24 hours and then concentrated to 4 μM (≈ 0.75 mL) using Millipore Centricon centrifugal filter devices (10 000 MWCO). Thereafter catalytic activity was measured and this was normalized (f_N) with the bigger activity value obtained.

4.7 Spectroscopic properties

Circular Dichroism (CD) experiments were carried out in buffer C in a Chirascan Spectropolarimeter (Applied Photophysics; Leatherhead, Surrey-UK) equipped with a Peltier device. CD spectra (180-250 nm wavelength range) were obtained with 20 μM BacTIM at 25 °C. Fluorescence measurements were made on a PC1 ISS Spectrofluorometer (Champaign, IL-USA) equipped with a Peltier and a water-jacketed cell holder for temperature control. The raw data were converted to molar ellipticity ([θ]) using the formula: [103] $[\theta] = \theta / (l*C*N_r)$ where θ is ellipticity in millidegrees, l is the cell path length in millimeters, C is the molar concentration of protein and N_r is the number of residues. Intrinsic fluorescence spectra of 8 μM BacTIM were determined in buffer C at 25 °C with 2 nm bandwidth slits with excitation at 295 nm and emission in the 310-410 nm range. The wavelength of maximal emission (λ_{max}) and fluorescence spectral center of mass (SCM) were calculated from intensity data (I_λ) obtained at different wavelengths: SCM $= \sum\lambda I_\lambda / \sum I_\lambda$.

4.8 Thermal transitions monitored by Circular Dichroism (CD) spectroscopy

Thermal unfolding and refolding transitions were followed using buffer C by monitoring ellipticity at 195 and 222 nm as a function of temperature at a heating rate of 1.0 K min^{-1}. Actual temperatures within the cell were registered with the external probe of the cell holder. Protein concentration ranged from 0.4 to 15 μM. 1.0 or 0.1 cm path-length cells were used accordingly. The changes in CD signal were analyzed after normalization of the transition curves to the fraction of unfolded molecules (f_D) by: $f_D = [y_{obs}-(y_N+m_N T)]/[(y_D+m_D T)-(y_N+m_N T)]$, where y_{obs} is the experimental observed DC signal at a given temperature and $(y_N+m_N T)$ and $(y_D+m_D T)$ are the fitting equations to straight lines representing the pre and post transition regions (native and unfolded states), respectively.

4.9 Thermal transitions monitored by Differential Scanning Calorimetry (DSC)

DSC experiments were done in a VP-Capillary DSC system (MicroCal, GE Healthcare). Protein concentration varied from 8 to 80 μM, and scan rates from 0.5 to 3.0 K min^{-1}. Protein solutions were prepared by exhaustive dialysis in buffer C and then degassed at room temperature. Buffer-buffer traces were subtracted from sample endotherms. For all proteins, a reheating run was carried out to determine the reversibility or irreversibility of the process. To verify that irreversibility was not the result of a too high final scanning temperature, first scans were also performed heating near the T_m. When irreversibility was observed, DSC traces were also obtained in the presence of urea (up to 2 M, where activity assays indicated the proteins remain in its dimer native state). Urea concentrations were determined from refractive index measurements. The Origin software package (MicroCal) was used for data analysis, calculation of unfolding enthalpies and ΔC_p determination.

4.10 Crystallization and data collection

All proteins were dialyzed in buffer B containing 100 mM NaCl. The hanging-drop vapor diffusion method was used to screen the crystallization conditions contained in the HR Crystal Screen I and II kits (Hampton Research). Crystals were obtained at 18 °C after incubating drops of proteins with the precipitant solutions in a 1:1 ratio. Crystallization conditions for the four BacTIMs were: for *Go*TIM 0.2 M potassium sodium tartrate, 0.1 M sodium citrate tribasic pH 5.6 and 2 M ammonium sulfate; for *Dr*TIM 1.8 M ammonium sulfate, 0.1 M sodium citrate tribasic pH 5.6 and 0.2 M potassium sodium tartrate; for *Sc*TIM 0.1 M TRIS hydrochloride pH 8.5 and 2.0 M ammonium sulfate; and for *Cp*TIM 0.2 M ammonium acetate, 0.1 M sodium acetate pH 4.6 and 30% w/v polyethylene glycol (PEG) 4000. For crystals obtained in conditions without PEG, a 30% w/v glycerol solution was used as cryoprotectant. Diffraction data were collected at 100 K with an oscillation of 0.5°/frame on an R-AXIS IV++ image plate detector (Rigaku, The Woodlands, TX) with X-rays (wavelength: 1.5418 Å) generated by a Rigaku MicroMax-007 HF rotating anode (Rigaku, The Woodlands, TX). All data sets were integrated using XDS[104] and scaled with SCALA in the CCP4 program suite v.6.1.2.[105]

4.11 Structure determination and refinement

All structures were solved by the molecular replacement method with PHASER in the PHENIX software suite.[106] *Thermotoga maritima* TIM (PDB ID: 1B9B), *Thermus thermophilus* TIM (PDB ID: 1YYA), *Mycobacterium tuberculosis* TIM (PDB ID: 3TA6) and *Geobacillus stearothermophilus* TIM (PDB ID: 1BTM) were used as the starting model for molecular replacement phasing of *Go*TIM (TFZ: 42.3 and log-likelihood gain: 1360.2), *Dr*TIM (TFZ: 32.8

and LLG: 1104.3), *Sc*TIM (TFZ: 45.6 and LLG: 3064.96) and *Cp*TIM (TFZ: 21.3 and LLG: 755.8), respectively. For all the structures, refinement was done with *phenix.refine*[106] and the models were improved by iteratively model rebuilding in COOT.[107] The final tridimensional structures were validated with MolProbity[108] and using the Protein Data Bank (PDB) validation server.[7] The coordinates and structure factors of *Go*TIM, *Dr*TIM, *Sc*TIM and *Cp*TIM have been deposited in the PDB under accession codes 4Y96, 4Y90, 4Y9A and 4Y8F, respectively. Table S2, ESI† summarizes data collection and refinement statistics. The figures were produced using PyMOL Molecular Graphics System, v1.7.2.[109]

4.12 Sequence and structural analysis

The sequence alignment was performed with MAFFT[110] and visually modified with Jalview.[111] Sequence identity percentage was calculated with SIAS server.[112] Nineteen dimeric structures for which their thermal unfolding have been studied (including those studied in this work) were selected for a structural comparison; the characteristics of these three-dimensional structures are summarized in Table S6, ESI†. Structural alignments were performed using UCSF Chimera[113] and PyMOL Molecular Graphics System, v1.7.2.[109] RMSD values were calculated with a distance matrix using GRASP.[114] The assignment and composition of secondary structure elements was determined with STRIDE.[115] Molecular volumes and cavities were calculated with the 3V software suite[116] and MOLE v2.13.9.6 software[117] using a random exploration path and a probe radius of 1.5 Å. A cavity was defined as an empty space buried inside the protein structure. The accessible surface area (ASA) and the difference in accessible surface area upon protein folding and assembly were calculated with PDBePISA v1.51,[118] Travel Depth[119] and NACCESS software[120] using a probe radius of 1.5 Å. Changes in ASA upon dissociation were calculated for a rigid body dissociation. For the unfolded state, accessibility was calculated using an extended Gly-X-Gly peptide with VADAR.[121] Hydrogen bonds between protein atoms were calculated using the HBPLUS[122] and VADAR routines with their default parameters for distances and angles. When two atoms of opposite charge were observed within 4 Å they were assigned to a salt bridge.

4.13 Data treatment and fitting

(i) Dissociation constant from the stability to dilution experiments. To obtain the dissociation constant for the dimer, K_{diss}, the normalized catalytic activity, $f_N(T)$, was plotted against protein concentration, P_c, and fitted to:

$$f_N(T) = \frac{K_{diss}(T) + 4P_c - \sqrt{K_{diss}(T)^2 + 8K_{diss}(T)P_c}}{4P_c} \quad (1)$$

(ii) Activation energy from the irreversible DSC transitions and kinetic and equilibrium urea m values. The shape of the calorimetric transitions is adequately described by the two-state irreversible model (N → F)[123,124] where N is the dimeric native protein, F is the final state (unable to fold back to the native protein). The kinetic conversion from N to F is described by a first-order rate constant (k) that changes with temperature according to the Arrhenius equation:

$$k = \exp\left[-\frac{E_A}{R}\left(\frac{1}{T} - \frac{1}{T^*}\right)\right] \quad (2)$$

where T^* is the temperature at which the k = 1 min^{-1}, and E_A is the activation energy from the native state to the transition state. The apparent heat capacity (corrected for the chemical baseline) in the two-state irreversible model is given by:

$$C_p^{APP} = \frac{\Delta H E_A}{RT_m^2}\exp(x) * \exp\left[-\exp(x)\right] \quad (3)$$

$$x = \frac{E_A}{RT_m^2}\left(T - T_m\right) \quad (4)$$

where T_m is the temperature corresponding to the maximum of the transition, T is the temperature at each point of the endotherm and ΔH is the unfolding enthalpy (consider a constant). The activation energies were obtained following three procedures. In the first, the DSC traces were fitted using eqns (3) and (4) at each of the employed scan rates, producing individual E_A values (one for each scan rate). In the second procedure, E_A is obtained from the slope of Arrhenius plots, *i.e.* ln k vs. 1/T, employing all scan rates. Finally, E_A can also be derived from a data consistency test, evaluating the effect of scanning rate (v) on T_m:[52]

$$\ln\left(\frac{v}{T_m^2}\right) = \text{constant} - \frac{E_A}{RT_m} \quad (5)$$

Kinetic urea m values ($m^{\ddagger}$) were used as a measure of exposure to the solvent (and, consequently, degree of unfolding) in the transition state.[125] They were obtained using:

$$m^{\ddagger} = -\frac{E_A}{T_m}\left(\frac{dT_m}{d[urea]}\right) - RT_m\left(\frac{d\ln\left(\frac{E_A}{RT_m}\right)}{d[urea]}\right) \quad (6)$$

The equilibrium m values (m_{eq}) were calculated using a correlation between m_{eq} and ΔASA.[73]

(iii) Enthalpy changes from the reversible CD and DSC transitions. The enthalpies from the native state to unfolded state, ΔH_{vH}, were obtained from a fit of the temperature dependence of the equilibrium constant within to the two-state reversible model,[126] $K_{eq} = (2f_D 2P_c)/(1\text{-}f_D)$, using the protein unfolded fraction (f_D) from CD data:

$$f_D = \frac{\left(y_N + m_N T\right) + \left(y_D + m_D T\right)\exp\left[\frac{\Delta H_{vH}}{R}\left(\frac{1}{T} - \frac{1}{T_m}\right)\right]}{1 + \exp\left[\frac{\Delta H_{vH}}{R}\left(\frac{1}{T} - \frac{1}{T_m}\right)\right]} \quad (7)$$

where T_m is the temperature corresponding to the 50% native and unfolded states.

The DSC endotherms were fitted to the equilibrium two-state model with dimer dissociation using (Microcal DSC data analysis tutorial guide v5.0):

$$C_p(T) = B_0 + B_1T + f(T)\Delta C_p + \frac{\Delta H_{cal}(T)}{RT_m^2}\left[\frac{1-f(T)}{-1+\frac{2}{f(T)}}\right] \quad (8)$$

where B_0 and B_1 are constants and $f(T)$ is the protein fraction in the monomer state, producing ΔH_{cal}, $\Delta C_{p,}$ and T_m. The van't Hoff enthalpy $\Delta H_{vH} = 4RT_{1/2}^2C_{p1/2}/\Delta H_{cal}$ with $T_{1/2}$ being the temperature where the fraction of native and unfolded proteins is 50%, and $C_{p1/2}$ the experimental heat capacity value at that temperature.

The enthalpy change $\Delta H'$ was also calculated from the dependence of T_m on protein concentration according to the Takahashi-Sturtevant equation:[127]

$$\ln P_c = b - \frac{\Delta H'}{RT_m} \quad (9)$$

with b being a constant, and T_m is the temperature corresponding to the 50% native and unfolded states.

(iv) Experimental, fitted and predicted heat capacity changes from the reversible DSC transitions. The experimental heat capacities for each protein concentration (ten of them) were converted into absolute heat capacities (Microcal DSC data analysis tutorial guide v5.0). The absolute heat capacity for the native state (C_{pN}) and unfolded state (C_{pD}) were fitted to straight lines and $\Delta C_p = C_{pD} - C_{pN}$ evaluated at the T_m (and then averaged). ΔC_p was also obtained as a fitted parameter using the equilibrium two-state model with dimer dissociation (eqn (8)). Finally, predicted ΔC_p values can be obtained from reported parametric equations, namely correlations based on amino acidic sequence and heat capacity changes,[68,69] and correlations between ΔASA and heat capacity changes.[70-74]

(v) Global stability curve. Stability curves, $\Delta G(T)$, were calculated using ΔH (ΔH_{cal}), ΔC_p and T_m obtained from eqn (8) and the Gibbs-Helmholtz equation:[128,129]

$$\Delta G(T) = \Delta H\left(1-\frac{T}{T_m}\right) - \Delta C_p\left(T_m - T + T\ln\left(\frac{T}{T_m}\right)\right) \quad (10)$$

Maximal stability occurs at a temperature T_S where $d\Delta G/dT = 0 = \Delta S$ *and* $\Delta H_{TS} = \Delta G(T_S)$.

5. Abbreviations

BacTIM, bacterial TIMs; CD, Circular Dichroism; *Cp*TIM, TIM from *Clostridium perfringens*; *Dr*TIM, TIM from *Deinococcus radiodurans*; DSC, Differential Scanning Calorimetry; E_A, activation energy; EukTIMs, eukaryotic TIMs; *Go*TIM, TIM from *Gemmata obscuriglobus*; Gnd-HCl, guanidinium hydrochloride; IrrevTIMs, TIMs with irreversible unfolding; *Np*TIM, TIM from *Nostoc punctiforme*; RevTIMs, TIMs with reversible unfolding; *Sc*TIM, TIM from *Streptomyces coelicolor*; TIM, Triosephosphate Isomerase; T_m, midpoint of thermal unfolding.

6. Acknowledgments

This work was supported by Consejo Nacional de Ciencia y Tecnología de México (Grant number 166472 to ARR, and 99857 to DAFV), Programa de Apoyo a Proyectos de Investigación e Innovación Tecnológica DGAPA-UNAM (PAPIIT grant number IN-112813 to MC, IN-207613 to ARR, and IN-219913 to DAFV), Facultad de Química and Facultad de Medicina, UNAM. SRR thanks Consejo Nacional de Ciencia y Tecnología de México (Grants numbers 313076 and 355134) and Posgrado en Ciencias Bioquímicas, UNAM, for financial support. We thank María Isabel Velázquez López and Georgina Espinosa Pérez for their competent technical support. X-Ray data were collected at the LANEM-IQ, UNAM. Conceived and designed the experiments: SRR MC ARR DAFV. Performed the experiments: SRR. Analyzed the data: SRR MC ARR DAFV. Contributed reagents/materials/analysis tools: MC ARR DAFV. Wrote the paper: SRR MC ARR DAFV. Performed the DSC experiments: SRR MC DAFV. Performed the crystallization and structural determination: SRR ARR. Project director: DAFV. All authors have given approval to the final version of the manuscript.

Dedications: *In memoriam* Prof. Armando Gómez-Puyou.

Conflict of Interest: The authors declare that they have no conflict of interest.

7. Notes and references

[1] Laboratorio de Fisicoquímica e Ingeniería de Proteínas, Departamento de Bioquímica, Facultad de Medicina, Universidad Nacional Autónoma de México, 04510 Ciudad de México, Distrito Federal, México. *E-mail: fdaniel@unam.mx

[2] Laboratorio de Biofisicoquímica, Departamento de Fisicoquímica, Facultad de Química, Universidad Nacional Autónoma de México, 04510 Ciudad de México, Distrito Federal, México.

[3] Laboratorio de Química de Biomacromoléculas 3, Departamento de Química de Biomacromoléculas, Instituto de Química, Universidad Nacional Autónoma de México, 04510 Ciudad de México, Distrito Federal, México.

† Electronic Supplementary Information (ESI) available. See DOI: 10.1039/b000000x/

1. K. A. Dill and J. L. MacCallum, *Science*, 2012, **338**, 1042-1046.
2. H. Feng, Z. Zhou and Y. Bai. *Proc. Natl. Acad. Sci., U. S. A*., 2005, **102**, 5026-5031.
3. N. Koga, R. Tatsumi-Koga, G. Liu, R. Xiao, T. B. Acton, G. T. Montelione and D. Baker, *Nature*, 2012, **491**, 222-227.
4. P. S. Huang, G. Oberdorfer, C. Xu, X. Y. Pei, B. L. Nannenga, J. M. Rogers, F. DiMaio, T. Gonen, B. Luisi and D. Baker, *Science*, 2014, **346**, 481-485.
5. D. A. Benson, M. Cavanaugh, K. Clark, I. Karsch-Mizrachi, D. J. Lipman, J. Ostell and E. W. Sayers, *Nucleic. Acids. Res.*, 2013, **41**, D36-D42.
6. H. M. Berman, J. Westbrook, Z. Feng, G. Gilliland, T. N. Bhat, H. Weissig, I. N. Shindyalov and P. E. Bourne, *Nucleic Acids Res*., 2000, **28**, 235-245.

7. M. D. Kumar, K. Abdulla-Bava, M. Michael-Gromiha, P. Prabakaran, K. Kitajima, H. Uedaira and A. Sarai, *Nucleic Acids Res*., 2005, **34**, D204-D206.
8. J. M. Scholtz, G. R. Grimsley, and C. N. Pace, *Meth. Enzymol.*, 2009, **466**, 549-565.
9. P. L. Privalov, *Adv. Protein Chem.,* 1979, **33**, 167-241.
10. J. M. Sanchez-Ruiz, *Annu. Rev. Phys. Chem*., 2011, **62**, 231-255.
11. C. M. Doyle, J. A. Rumfeldt, H. R. Broom, A. Broom, P. B. Stathopulos, K. A. Vassall, J. J. Almey and E. M. Meiering, *Arch. Biochem. Biophys*., 2013, **531**, 44-64.
12. E. Braselman, J. L. Chaney and P. L. Clark, *Trends Biochem. Sci.,* 2013, **38**, 337-344.
13. D. S. Goodsell and A. J. Olson, *Annu. Rev. Biophys. Biomol. Struct.*, 2000, **29**, 105-153.
14. R. Sterner and B. Höcker, *Chem. Rev*., 2005, **105**, 4038-4055.
15. R. K. Wierenga, R. K. *FEBS Lett*., 2001, **492**, 193-198.
16. N. Nagano, C. A. Orengo and J. M. Thornton, *J. Mol. Biol*., 2002, **321**, 741-765.
17. W. R. Forsyth and C. R. Matthews, *J. Mol. Biol*., 2002, **320**, 1119-1133.
18. L. Carstensen, J. M. Sperl, M. Bocola, F. List, F. X. Schmid and R. Sterner, *J. Am. Chem. Soc*., 2012, **134**, 12786-12791.
19. B. N. Gangadhara, J. M. Laine, S. V. Kathuria, F. Massi and C. R. Matthews, *J. Mol. Biol*., 2013, **425**, 1065-1081.
20. R. Rudolph, R. Siebendritt and T. Kiefhaber, *Protein Sci*., 1992, **1**, 654-666.
21. A. A. Moosavi-Movahedi, B. Samiee and G. H. Hakimelahi, *J. Colloid Interf. Sci*., 1993, **161**, 53-56.
22. S. Pyrpassopoulos, M. Vlassi, A. Tsortos, Y. Papanikolau, K. Petratos, C. E. Vorgias and G. Nounesis, *Proteins*, 2006, **64**, 513-523.
23. V. Mainfroid, S. C. Mande, W. G. J. Hol, J. Martial and K. Goraj, *Biochemistry*, 1996, **35**, 4110-4117.
24. A. W. Rietveld and S. T. Ferreira, *Biochemistry*, 1996, **35**, 7743-7751.
25. N. Beaucamp, A. Hofmann, B. Kellerer and R. Jeanicke, *Protein Sci*., 1997, **6**, 2159-2165.
26. A. W. Rietveld and S. T. Ferreira, *Biochemistry*, 1998, **37**, 933-937.
27. R. S. Gokhale, S. S. Ray, H. Balaram and P. Balaram, *Biochemistry*, 1999, **38**, 423-431.
28. A. M. Lambeir, J. Backmann, J. Ruiz-Sanz, V. Filimonov, J. E. Nielsen, I. Kursula, B. V. Norledge and R. K. Wierenga, *Eur. J. Biochem*., 2000, **267**, 2516-2524.
29. C. J. Morgan, D. K. Wilkins, L. J. Smith, Y. Kawata and C. M. Dobson, *J. Mol. Biol*., 2000, **300**, 11-16.
30. M. E. Chánez-Cárdenas, D. A. Fernández-Velasco, E. Vázquez-Contreras, R. Coria-Ortega, G. Saab-Rincón and R. Pérez-Montfort, *Arch. Biochem. Biophys*., 2002, **399**, 117-129.
31. V. H. Moreau, A. W. Rietveld and S. T. Ferreira, *Biochemistry*, 2003, **42**, 14831-14837.
32. H. Nájera, M. Costas and D. A. Fernández-Velasco, *Biochem. J.*, 2003, **370**, 785-792.
33. H. Pan, A. S. Raza and D. L. Smith, *J. Mol. Biol*., 2004, **336**, 1251-1263.
34. M. E. Chánez-Cárdenas, G. Pérez-Hernández, B. G. Sánchez-Rebollar, M. Costas and E. Vázquez-Contreras, *Biochemistry*, 2005, **44**, 10883-10892.
35. A. R. Vázquez-Pérez and D. A. Fernández-Velasco, *Biochemistry*, 2007 **46**, 8624-8633.
36. Y. Shi, J. H. Liu, H. J. Zhang and Y. Ding, *Protein Pept. Lett*., 2008, **15**, 365-370.
37. V. Guzman-Luna and G. Garza-Ramos, *Proteins*, 2012, **80**, 1669-1682.
38. S. Lara-González, P. Estrella-Hernández, A. Ochoa-Leyva, M. Del Carmen Portillo-Téllez, L. A. Caro-Gómez, E. E. Figueroa-Angulo, H. Salgado-Lugo, J. F. T. Miranda-Ozuna, J. Ortega-López, R. Arroyo, L. G. Brieba and C. B. Benítez-Cardoza, *Proteins*, 2014, **82**, 22-33.
39. J. R. Knowles, *Nature*, 1991, **350**, 121-124.
40. J. P. Richard, *Biochemistry*, 2012, **51**, 2652-2661.
41. D. Maes, J. P. Zeelen, N. Thanki, N. Beaucamp, M. Alvarez, M. H. Thi, J. Backmann, J. A. Martial, L. Wyns, R. Jaenicke and R. K. Wierenga, *Proteins*, 1999, **37**, 441-453.
42. M. Peimbert, L. Domínguez-Ramírez, L. A. Téllez, L. M. Blancas and D. A. in *Advances in Protein Physical Chemistry*, ed. E. García-Hernández and D. A. Fernández-Velasco, Transworld Research Network, Kerala, 1st edn., 2008, vol. 1, ch. 11, pp. 193-217.
43. A. Sun, Q. K. U. Yuksel and R. W. Gracy, *Arch. Biochem. Biophys*., 1995, **322**, 361-368.
44. M. Alvarez, J. P. Zeelen, V. Mainfroid, F. Rentier-Delrue, J. A. Martial, L. Wyns, R. K. Wierenga and D. Maes, *J. Biol. Chem*., 1998, **273**, 2199-2206.
45. M. Alvarez, J. Wouters, D. Maesi, V. Mainfroid, F. Rentier-Delrue, L. Wyns, E. Depiereux and J. A. Martial, *J. Biol. Chem*., 1999, **274**, 19181-19187.
46. S. S. Ray, H. Balaram and P. Balaram, *Chem. Biol*., 1999, **6**, 625-637.
47. C. G. Benítez-Cardoza, A. Rojo-Domínguez and A. Hernández-Arana, *Biochemistry*, 2001, **40**, 9049-9058.
48. L. Jiménez, D. A. Fernández-Velasco, K. Willms and A. Landa, *J. Parasitol.*, 2003, **89**, 209-214.
49. D. Mathur, G. Malik and L. C. Garg, *FEMS Microbiol. Lett*., 2006, **263**, 229-235.
50. S. Enríquez-Flores, A. Rodríguez-Romero, G. Hernández-Alcántara, J. Oria-Hernández, P. Gutiérrez-Castrellón, G. Pérez-Hernández, I. de la Mora-de la Mora, A. Castillo-Villanueva, I. García Torres, S. T. Méndez, S. Gómez-Manzo, A. Torres-Arroyo, G. López-Velázquez and H. Reyes-Vivas, *Proteins*, 2007, **79**, 2711-2724.
51. L. A. Téllez, L. M. Blancas-Mejía, E. Carrillo-Nava, G. Mendoza-Hernández, D. A. Cisneros and D. A. Fernández-Velasco, *Biochemistry*, 2008, **47**, 11665-11673.
52. M. Costas, D. Rodríguez-Larrea, L. De Maria, T. V. Borchert, A. Gómez-Poyou and J. M. Sanchez-Ruiz, *J. Mol. Biol*., 2009, **385**, 924-937.
53. Y. Aguirre, N. Cabrera, B. Aguirre, R. Pérez-Montfort, A. Hernandez-Santoyo, H. Reyes-Vivas, S. Enríquez-Flores, M. T. de Gómez-Puyou, A. Gómez-Puyou, J. M. Sanchez-Ruiz and M. Costas, *Proteins*, 2014, **82**, 323-335.
54. T. Cavalier-Smith, *Biol Direct*., 2006, **1**, 1-19.
55. J. R. Lakowicz, in *Principles of Fluorescence Spectroscopy*, Springer, New York, 3rd edn., 2006, vol. 1, ch. 16, pp. 529-575.
56. V. Mainfroid, P. Terpstra, M. Beauregard, J. M. Frère, S. C. Mande, W. G. J. Hol, J. A. Martial and K. Goraj, *J. Mol. Biol*., 1996, **257**, 441-456.

57. A. Landa, A. Rojo-Domínguez, L. Jiménez and D. A. Fernández-Velasco, *Eur. J. Biochem*., 1997, **247**, 348-355.
58. H. Reyes-Vivas, E. Martínez-Martínez, G. Mendoza-Hernández, G. López-Velázquez, R. Pérez-Montfort, M. T. de Gómez-Puyou and A. Gómez-Puyou, *Proteins*, 2002, **48**, 580-590.
59. G. López-Velázquez, D. Molina-Ortíz, N. Cabrera, G. Hernández-Alcántara, J. Peón-Peralta, L. Yépez-Mulia, R. Pérez-Montfort, H. Reyes-Vivas, *Proteins*, 2004, **55**, 824-834.
60. H. Reyes-Vivas, A. Díaz, J. Peón, G. Mendoza-Hernández, G. Hernández-Alcántara, I. de la Mora-de la Mora, S. Enríquez-Flores, L. Domínguez-Ramírez and G. López-Velázquez, *J. Mol. Biol*., 2007, **365**, 752-763.
61. D. R. Trentham, C. H. McMurray and C. I. Pogson, *Biochem. J*., 1969, **114**, 19-24.
62. G. Böhm, R. Muhr and R. Jaenicke, *Protein Eng*., 1992, **5**, 191-195.
63. N. Sreerama and R. W. Woody, *Meth. Enzymol*., 2004, **383**, 318-351.
64. L. Whitmore and B. A. Wallace, *Biopolymers*, 2008, **89**, 392-400.
65. C. Vita, A. Fontana, J. R. Seeman and I. M. Chaiken, *Biochemistry*, 1979, **18**, 3023-3031.
66. L. López-Arenas, S. Solís-Mendiola and A. Hernández-Arana, *Biochemistry*, 1999, **38**, 15936-15943.
67. E. Freire, *Comments Mol. Cell Biophys*., 1989, **6**, 123-140.
68. D. Milardi, C. la Rosa, S. Fasone and D. Grasso, *Biophys. Chem*., 1997, **69**, 43-51.
69. A. D. Robertson and K. P. Murphy, *Chem. Rev*., 1997, **97**, 1251-1267.
70. K. P. Murphy and E. Freire, *Adv. Protein Chem*., 1992, **43**, 313-361.
71. R. S. Spolar and M. T. Record, *Science*, 1994, **263**, 777-784.
72. G. I. Makhatadze and P. L. Privalov, *Adv. Protein Chem*., 1995, **47**, 307-425.
73. J. K. Myers, C. N. Pace and J. M. Scholtz, *Protein Sci*., 1995, **4**, 2138-2148.
74. B. Madan and K. A. Sharp, *Biophys. J*., 2001, **81**, 1881-1887.
75. D. C. Rees and A. D. Robertson, *Protein Sci.*, 2001, **10**, 1187-1194.
76. K. M. Hart, M. J. Harms, B. H. Schmidt, C. Elya, J. W. Thornton and S. Marqusee, *PLoS Biol*., 2014, **12**, 1-12.
77. R. G. E. Murray, in *The prokaryotes*, ed. A. Balows, H. G. Trüper, M. Dworkin, W. Harder and K. H. Schleifer, Springer-Verlag, New York, 2nd edn.,1992, vol. 4, ch. 204, pp. 3732-3744.
78. J. Bursy, A. U. Kuhlmann, M. Pittelkow, H. Hartmann, M. Jebbar, A. J. Pierik and E. Bremer, *Appl. Environ. Microbiol*., 2008, **74**, 7286-7296.
79. J. Li and B. A. McClane, *Appl. Environ. Microbiol*., 2006, **72**, 4561-4568.
80. E. Gasteiger, C. Hoogland, A. Gattiker, S. Duvaud, M. R. Wilkins, R. D. Appel and A. Bairoch, in *The Proteomics Protocols Handbook*, ed. J. M. Walker, Humana Press, New York, 1st edn., 2005, vol. 1, ch. 52, pp. 571-607.
81. V. D. Trivedi, B. Raman, C. M. Rao and T. Ramakrishna, *FEBS Lett.*, 1997, **418**, 363-366.
82. A. Fersht, in Structure and mechanism in protein science: a guide to enzyme catalysis and protein folding, Freeman, New York, 1st edn., 1999, vol. 1, ch. 17, pp. 508-539.
83. K. Shiraki, M. Kudou, S. Fujiwara, T. Imanaka and M. Takagi, *J. Biochem.*, 2002, **132**, 591-595.
84. J. L. Silva and G. Weber, *Annu. Rev. Phys. Chem*., 1993, **44**, 89-113.
85. J. Roche, M. Dellarole, J. A. Caro, D. R. Norberto, A. E. Garcia, B. Garcia-Moreno, C. Roumestand and C. A. Royer, *J. Am. Chem. Soc*., 2013, **135**, 14610-14618.
86. E. Mixcoha-Hernández, L. M. Moreno-Vargas, A. Rojo-Domínguez and C. G. Benítez-Cardoza, *Protein J*., 2007, **26**, 491-498.
87. H-J. Woo and B. Roux, *Proc. Natl. Acad. Sci., U. S. A*., 2005, **102**, 6825-6830.
88. D. Li, B. Ji, K. Hwang and Y. Huang, *PLoS One*, 2011, **6**, e19268.
89. L. S. Cheung, D. J. Shea, N. Nicholes, A. Date, M. Ostermeier and K. Konstantopoulos, *Sci. Rep.*, 2015, **5**, 1-9.
90. L. A. Abriata and M. Dal Peraro. *Sci. Rep.*, 2015, **5**, 1-12.
91. J. M. Sanchez-Ruiz, *Biophys. Chem*., 2010, **148**, 1-15.
92. J. Gomes and W. Steiner, *Food Technol. Biotechnol.*, 2004, **42**, 223-235.
93. A. Bhattacharya and B. I. Pletschke, *Enzyme Microb. Technol*., 2014, **55**, 159-169.
94. S. Lindquist, *Ann. Rev. Biochem*., 1986, **55**, 1151-1191.
95. A. Muga and F. Moro, *Curr. Protein Pept. Sci*., 2008, **9**, 522-566.
96. M. J. Gething and J. Sambrook, *Nature*, 1992, **355**, 33-45.
97. N. A. Ryabova, V. V. Marchenkov, S. Y. Marchenkova, N. V. Kotova and G. V. Semisotnov, *Biochemistry Mosc.*, 2013, **78**, 1405-1414.
98. P. Bozaykut, N. K. Ozer and B. Karademir, *Free Radic. Biol. Med*., 2014, **77**, 195-209.
99. M. J. Kerner, D. J. Naylor, Y. Ishihama, T. Maier, H. C. Chang, A. P. Stines, C. Georgopoulos, D. Frishman, M. Hayer-Hartl, M. Mann and F. Urlrich, *Cell*, 2005, **122**, 209-220.
100. F. D. Ciccarelli, T. Doerks, C. von Mering, C. J. Creevey, B. Snel, and P. Bork, *Science*, 2006, **311**, 1283-1287.
101. K. Guruprasad, B. V. Reddy and M. W. Pandit, *Protein Eng*., 1990, **4**, 155-161.
102. V. N. Uversky, *Biochemistry*, 1993, **32**, 13288-13298.
103. N. J. Greenfield, *Nat. Protoc*., 2006, **1**, 2876-2890.
104. W. Kabsch, *Acta Crystallogr. Sect. D*., 2010, **66**, 125-132.
105. M. D. Winn, C. C. Ballard, K. D. Cowtan, E. J. Dodson, P. Emsley, P. R. Evans, R. M. Keegan, E. B. Krissinel, A. G. W. Leslie, A. McCoy, S. J. McNicholas, G. N. Murshudov, N. S. Pannu, E. A. Potterton, H. R. Powell, R. J. Read, A. Vagin and K. S. Wilson, *Acta Crystallogr. Sect. D*., 2011, **67**, 235-242.
106. P. A. Adams, P. V. Afonine, G. Bunkóczi, V. B. Chen, I. W. Davis, N. Echols, J. J. Headd, L. W. Hung, G. J. Kapral, R. W. Grosse-Kunstleve, A. J. McCoy, N. W. Moriarty, R. Oeffner, R. J. Read, D. C. Richardson, J. S. Richardson, T. C. Terwilliger and P. H. Zwart, *Acta Cryst. Sect. D.*, 2010, **66**, 213-221.
107. P. Emsley and K. Cowtan, *Acta Crystallogr. Sect. D*., 2004, **60**, 2126-2132
108. I. W. Davis, A. Leaver-Fay, V. B. Chen, J. N. Block, G. J. Kapral, X. Wang, L. W. Murray, W. B. Arendall III, J. Snoeyink, J. Richardson and D. C. Richardson, *Nucleic Acids Res*., 2007, **35**, W375-W383.
109. The PyMOL Molecular Graphics System, version 1.7.2, Schrödinger, LLC, New York, U.S., 2014.
110. K. Katoh and D. M. Standley, *Mol. Biol. Evol*., 2013, **30**, 772-780.
111. A. M. Waterhouse, J. B. Procter, D. M. A. Martin and G. J. Barton, *Bioinformatics*, 2009, **25**, 1189-1191.
112. P. Reche, SIAS, Universidad Complutense de Madrid, Madrid, Spain, 2013.

113. E. F. Pettersen, T. D. Goddard, C. C. Huang, G. S. Couch, D. M. Greenblatt, E. C. Meng, and T. E. Ferrin, *J. Comput. Chem*., 2004, **25**, 1605-1612.
114. A. Nicholls, K. A. Sharp and B. Honig, *Proteins*, 1991, **11**, 281-296.
115. M. Heinig and D. Frishman, *Nucleic Acids Res*., 2004, **32**: W500-W502.
116. N. R. Voss and M. Gerstein, *Nucleic Acids Res*., 2010, **38**: W555-W562.
117. K. Berka, O. Hanák, D. Sehnal, P. Banás, V. Navrátilová, D. Jaiswal, C. M. Ionescu, R. Svobodová, J. Koca and M. Otyepka, *Nucleic Acids Res.*, 2012, **40**, W222-W227.
118. E. Krissinel and K. Henrick, *J. Mol. Biol*., 2007, **372**: 774-797.
119. R. G. Coleman and K. A. Sharp, *J. Mol. Biol*., 2006, **362**, 441-458.
120. S. J. Hubbard and J. M. Thornton, NACCESS, University College London, London, U. K., 1993.
121. L. Willard, A. Ranjan, H. Zhang, H. Monzavi, R. F. Boyko, B. D. Sykes and D. S. Wishart, *Nucleic Acids Res*., 2003, **31**, 3316-3319.
122. I. McDonald and J. Thornton, *J. Mol. Biol*., 1994, **238**, 777-793.
123. J. M. Sanchez-Ruiz, *Biophys. J.*, 1992, **61**, 921-935.
124. A. E. Lyubarev and B. I. Kurganov, *Biochemistry Mosc*., 1998, **63**, 434-440.
125. D. Rodríguez-Larrea, S. Minning, T. V. Borchert and J. M. Sanchez-Ruiz, *J. Mol. Biol*., 2006, **360**, 715-724.
126. C. N. Pace, B. A. Shirley and J. A. Thomson, in *Protein structure: a practical approach*, ed. T. E. Creighton, IRL Press, Oxford, 2nd edn., 1997, vol. 1., ch. 12, pp. 311-330.
127. K. Takahashi and J. M. Sturtevant, *Biochemistry*, 1981, **20**, 6185-6190.
128. M. M. Santoro and D. W. Bolen, *Biochemistry*, 1992, **31**, 4901-4907.
129. S. Kumar, C. J. Tsai and R. Nussinov, *Biochemistry*, 2002, **41**, 5359-5374.